Frontiers of Information Technology & Electronic Engineering
www.jzus.zju.edu.cn; engineering.cae.cn; www.springerlink.com
ISSN 2095-9184 (print); ISSN 2095-9230 (online)
E-mail: jzus@zju.edu.cn

Enhancing modelling accuracy of cascaded spline adaptive filters using the remora optimisation algorithm: application to real-time systems#

Lakshminarayana JANJANAM‡[1], Suman Kumar SAHA[2], Rajib KAR[3]

[1]*JNTUK Recognized Research Center, Department of Electronics & Communication Engineering, Sasi Institute of Technology & Engineering, Andhra Pradesh 534101, India*

[2]*Department of Electronics & Communication Engineering, National Institute of Technology Raipur, Chhattisgarh 492010, India*

[3]*Department of Electronics & Communication Engineering, National Institute of Technology Durgapur, West Bengal 713209, India*

E-mail: jlphd.nitrr@gmail.com; namus.ahas@gmail.com; rajibkarece@gmail.com

Received Dec. 3, 2023; Revision accepted Mar. 21, 2024; Crosschecked Apr. 17, 2024

Abstract: We first introduce a new approach for optimising a cascaded spline adaptive filter (CSAF) to identify unknown nonlinear systems by using a meta-heuristic optimisation algorithm (MOA). The CSAF architecture combines Hammerstein and Wiener systems, where the nonlinear blocks are implemented with the spline network. The algorithms used optimise the weights of the spline interpolation function and linear filter by using an adequately weighted cost function, leading to improved filter stability, steady state performance, and guaranteed convergence to globally optimal solutions. We investigate two CSAF architectures: Hammerstein–Wiener SAF (HW-SAF) and Wiener–Hammerstein SAF (WH-SAF) structures. These architectures have been designed using gradient-based approaches which are inefficient due to poor convergence speed, and produce suboptimal solutions in a Gaussian noise environment. To avert these difficulties, we estimate the design parameters of the CSAF architecture using four independent MOAs: differential evolution (DE), brainstorm optimisation (BSO), multi-verse optimiser (MVO), and a recently proposed remora optimisation algorithm (ROA). In ROA, the remora factor's control parameters produce near-global optimal parameters with a higher convergence speed. ROA also ensures the most balanced exploration and exploitation phases compared to DE-, BSO-, and MVO-based design approaches. Finally, the identification results of three numerical and industry-specific benchmark systems, including coupled electric drives, a thermic wall, and a continuous stirred tank reactor, are presented to emphasise the effectiveness of the ROA-based CSAF design.

Key words: Cascaded spline adaptive filter; Nonlinear system identification; Remora optimisation algorithm
https://doi.org/10.1631/FITEE.2300817 **CLC number:** O231

1 Introduction

The adaptive filtering technique is extensively applied to solve various engineering problems in the signal processing field, such as active noise control (Raja et al., 2018), system identification (Zhang et al., 2021), channel estimation and equalisation (Zhang et al., 2021), noise cancellation (Yadav et al., 2022), and echo cancellation (Sankar et al., 2020). The use of the technique is well-established for system identification problems due to its versatility in many design-oriented accurate word problems. The primary linear adaptive filter performs better if the plant exhibits linear characteristics, producing unacceptable results (Janjanam et al., 2021a). In general, real systems are nonlinear. Hence, designing a nonlinear system to handle such nonlinearity is essential. Many identification models for nonlinear plant identification (Janjanam et al., 2021a) are described below.

‡ Corresponding author

Electronic supplementary materials: The online version of this article (https://doi.org/10.1631/FITEE.2300817) contains supplementary materials, which are available to authorized users

ORCID: Lakshminarayana JANJANAM, https://orcid.org/0000-0001-5340-4058

The Volterra filter (Janjanam et al., 2021b; Wang et al., 2022) and its improved variant, the kernel adaptive filter (KAF) (Garcia-Vega et al., 2020), are nonlinear filters that are widely used to characterise any nonlinearity theoretically. However, their computational complexity (CC) is too high and many parameters are required. Although the neural network (NN) (Jia L and Feng, 2017; Chen et al., 2022) is simple and flexible to design the system, it has high CC and quickly becomes trapped in local optimal solutions. The functional link artificial neural network (FLANN) (Patel et al., 2016) is another efficient model for nonlinear plant modelling that has the structure of a higher order Volterra series with low CC. However, the identification accuracy and CC of the FLANN depend on the nature of the function used for input signal expansion.

Chaudhary et al. (2019) noted that different kinds of block-oriented models (BOMs) are used to represent nonlinear systems, especially industry-specific plants. A BOM consists of a combination of linear dynamic filters and nonlinear static functions. The primary classes of BOMs are Hammerstein and Wiener models. The series connection of a nonlinear function and linear filter forms the structure of the Hammerstein model (Chaudhary et al., 2019; Mehmood et al., 2019a, 2019b; Janjanam et al., 2022b). Janjanam et al. (2022b) identified various Hammerstein benchmark plants using the social mimic optimisation algorithm assisted Kalman filter, and successfully estimated the state of the heating system and cascaded tanks. Moreover, Mehmood et al. (2019a, 2019b) enforced the backtracking search optimisation algorithm for Hammerstein model tracking (Mehmood et al., 2019b) and modelled the electrical muscle system based on the Hammerstein model (Mehmood et al., 2019a).

In contrast, a Wiener model is formed by a cascading linear filter that is succeeded by a nonlinear function (Pal et al., 2017; Janjanam et al., 2022d). Various evolutionary techniques, namely brainstorm optimisation (BSO) (Pal et al., 2017) and moth-flame optimisation (Janjanam et al., 2022d) algorithms, are used for the tracking of standard Wiener system outputs and produce better results than other reported methods (Janjanam et al., 2022d). Meta-heuristic optimisation algorithms (MOAs) can solve highly complex and multidisciplinary problems. Jia HM et al. (2023) proposed a crayfish optimisation algorithm and used it to optimise complex CEC2014 benchmark test functions and to solve design problems of various practical systems, such as a tension/compression spring, welded beam, and pressure vessel. Dynamic Harris hawks optimisation with a mutation algorithm (Jia HM et al., 2019) was successfully used for segmentation of satellite images. Xu et al. (2019) successfully used a hybrid dragonfly algorithm and differential evolution algorithms for multilevel colour image segmentation. The above discussion confirms that MOAs can be used to efficiently identify complex and multidimensional systems and derive near-global optimal coefficients with a high convergence speed compared to other approaches. Hence, we use MOAs in this study to estimate cascaded spline adaptive filters (CSAFs).

Unfortunately, Hammerstein and Wiener models individually do not guarantee good identification results for practical design-oriented problems (Li LW and Ren, 2018). Hence, a cascade of the above models is used. In earlier studies (Li LW and Ren, 2018; Janjanam et al., 2022c), the outputs of a turntable servo system (Li LW and Ren, 2018) and real-time nonlinear electronic system (Janjanam et al., 2022c) were effectively tracked using one of the most popular cascaded architectures, called the Wiener–Hammerstein (WH) model. The WH model gives the best results in the presence of noise (Esmaeilani et al., 2021; Liu Q et al., 2021). In practical plants, namely the ball-and-beam and robot arm systems, Janjanam et al. (2022a) used an optimally tuned Sage–Husa adaptive Kalman filter based on another cascaded structure called Hammerstein–Wiener (HW).

Recently, the parameters of various highly nonlinearity-oriented HW plants were identified using Levenberg–Marquardt (Hammar et al., 2019) and weighted differential evolution (Mehmood and Raja, 2023) algorithms. However, the methods proposed for cascaded model identification (Li LW and Ren, 2018; Hammar et al., 2019; Esmaeilani et al., 2021; Janjanam et al., 2022a) were improved versions of gradient-based approaches characterised by low convergence speed and moderate estimation accuracy. Moreover, very few studies (Janjanam et al., 2022a, 2022c; Mehmood and Raja, 2023) have used MOA-based methods. Hence, in this study, we focus only on a cascaded model with efficient MOAs. In addition,

the tracking accuracy of HW and WH models depends on the type of nonlinearity used in the nonlinear function blocks (Li LW and Ren, 2018). Recent studies (Scarpiniti et al., 2014; Gao et al., 2023) have confirmed that spline nonlinearity gives better identification accuracy than other nonlinearities such as polynomials and piece-wise linear functions.

Spline adaptive filters (SAFs) have recently attracted increasing attention because of their higher accuracy, simplicity, and flexibility in implementation, and lower CC. They have been used in numerous applications such as unknown system modelling (Scarpiniti et al., 2014), nonlinear active noise control (Gao et al., 2023), and channel estimation in wireless sensor network applications (Mishra et al., 2023). A series of intriguing studies on SAFs for nonlinear system identification have been published. Various SAF architectures have been developed such as Hammerstein SAF (HSAF) (Scarpiniti et al., 2014), Wiener SAF (WSAF) (Scarpiniti et al., 2013, 2015a), and cascaded SAFs (HW-SAF and WH-SAF) (Scarpiniti et al., 2015b, 2018) based on the least mean square (LMS) algorithm for effective modelling of nonlinear plants. Moreover, the robustness of these SAFs has been investigated under different signal-to-noise ratio (SNR) conditions. Yang et al. (2019) and Yu et al. (2021) proposed other unique cost functions and modified stochastic gradient techniques to improve the robustness of SAF against noise.

To reduce the effect of impulse noise, researchers have designed SAFs using different techniques such as the generalised maximum Versoria criterion (GMVC) algorithm (Guo and Zhi, 2022), Heaviside step function (Guan et al., 2022), and arctangent-exponential hyperbolic cosine (Guo et al., 2022). In addition, Liu C and Zhao (2023) proposed a complex valued SAF based on a two-dimensional look-up table (LUT), yielding good estimation results with low CC. Li WQ et al. (2023) developed a frequency domain SAF based on a half-quadratic criterion (HQC), offering better robustness and low CC. Guan and Biswal (2023) proposed SAF-Adagrad and SAF-RMSProp methods to improve convergence and steady-state performance in nonlinear system modelling.

Recently, Gao et al. (2024) developed a q-gradient LMS with a variable step size algorithm for the design of SAF. This technique further balances the convergence rate and steady-state error and deals with deficiency due to a constant step size. Yu et al. (2024) effectively designed a robust sub-band HSAF with exponential, hyperbolic cosine fitness functions and used it to solve system identification and acoustic echo cancellation problems. However, the SAFs mentioned above are modelled with stochastic gradient approaches, which easily traverse to locally optimal solutions and take a considerable number of epochs (the order of 10^4) to converge, and the accuracy depends on the initial parameter setting. Moreover, existing techniques have been developed based on some prior assumptions, leading to high algorithm complexity and producing low-quality solutions when dealing with a higher data rate and practical systems (Scarpiniti et al., 2015b, 2018). MOA is the only solution considered here to address these problems.

Janjanam et al. (2023) have proposed a novel methodology to solve the design problem of HSAF using MOA. They proposed an efficient cost function minimised with the snake optimiser algorithm (SOA) by simultaneously amending the design parameters of HSAF, such as the linear filter coefficients and the weights of spline control points. Their experimental results confirmed that the MOA-based design approach derives the global optimal HSAF coefficients and improves the filter convergence speed and stability compared with previous methods (Janjanam et al., 2023). Based on the knowledge gained from their study, in this article, we present two distinct CSAFs (HW-SAF and WH-SAF) successfully designed for nonlinear system modelling using an efficient MOA called the remora optimisation algorithm (ROA).

The main contributions of this article are as follows:

1. We introduce the novel application of MOAs through ROA, multi-verse optimiser (MVO), BSO, and differential evolution (DE) algorithms for reliable, accurate, and robust estimation of CSAF nonlinear systems (WH-SAF and HW-SAF). Moreover, we analyse their performance by varying the noise level from low to high.

2. The outcomes of several independent tests are analysed to estimate the stability of the methodology.

3. Holm's hypothesis test is applied to compare the consistency of the proposed ROA-based design with that of other designs.

4. The estimation accuracy of the proposed scheme is verified with mean absolute error (MAE), root mean squared deviation (RMSD), mean weight deviation (MWD), and Thiel's inequality coefficient (TIC) metrics.

5. The potency of the WH-SAF and HW-SAF models over other most familiar identification models for nonlinear system design is explored and the complexity of the proposed method is discussed.

6. The identification problem of three real-life benchmark systems is examined.

2 Problem description

SAF's basic theory and working principles are available in Scarpiniti et al. (2013, 2014). In this section, we derive the measurement forms and cost functions of the chosen models.

2.1 Mathematical modelling of HW-SAF and its cost function formulation

A schematic of an HW-SAF is shown in Fig. 1, where a linear filter (LF) is sandwiched between two memoryless nonlinear static functions, which are implemented with the SAF architecture (Scarpiniti et al., 2015b). The NSAF structure consists of a nonlinear network of an adaptable LUT and a spline interpolator. Fig. 1 shows that at time instant n, the signals $u[n]$ and $y[n]$ are the system's input and output, respectively. The symbols of NSAF 1 and NSAF 2 blocks are denoted by superscripts 1 and 2, respectively.

Step 1: mathematical modelling of NSAF 1

The nonlinear relationship between the signals $u[n]$ and $g[n]$ of NSAF 1 is expressed as $g[n]=f^{(1)}(u[n], \boldsymbol{r}_{i,n}^{(1)})$ (Scarpiniti et al., 2015b), where $f^{(1)}(\cdot)$ denotes the nonlinear spline function of NSAF 1, which is a smooth curve interpolated by the definite length of control points in the LUT, and the variable $\boldsymbol{r}_{i,n}^{(1)}$ is the spline control point vector represented by $\boldsymbol{r}_{i,n}^{(1)}\in\mathbb{R}^{4\times 1}=[\, r_{i,n}^{(1)}, r_{i+1,n}^{(1)}, r_{i+2,n}^{(1)}, r_{i+3,n}^{(1)}\,]^{\mathrm{T}}$. The spline estimation is based on the local parameter ρ and span index i. The calculation of these two parameters for NSAF 1 at time instant n is given as (Scarpiniti et al., 2015b)

$$\begin{cases} i_n^{(1)} = \lfloor u[n]/\Delta u^{(1)} \rfloor + (R^{(1)} - 1)/2, \\ \rho_n^{(1)} = u[n]/\Delta u^{(1)} - \lfloor u[n]/\Delta u^{(1)} \rfloor, \end{cases} \tag{1}$$

where $\Delta u^{(1)}$ is the sampling interval between the control points, $\lfloor\cdot\rfloor$ is the floor operator, and $R^{(1)}$ denotes the total number of control points.

The response $g[n]$ of NSAF 1 block for the input $u[n]$ is mathematically expressed as

$$g[n]=\left(\boldsymbol{\rho}_{i,n}^{(1)}\right)^{\mathrm{T}}\boldsymbol{C}\boldsymbol{r}_{i,n}^{(1)}, \tag{2}$$

where $\boldsymbol{\rho}_{i,n}^{(1)}\in\mathbb{R}^{4\times 1}=[\,\rho_{i,n}^{3(1)}, \rho_{i,n}^{2(1)}, \rho_{i,n}^{(1)}, 1\,]^{\mathrm{T}}$ and the pre-measured 4×4 spline basis matrix $\boldsymbol{C}$ is either B-spline $\boldsymbol{C}_{\mathrm{B}}$ or Catmull–Rom (CR) spline $\boldsymbol{C}_{\mathrm{CR}}$ (Scarpiniti et al., 2013) as given in Eq. (3):

$$\boldsymbol{C}_{\mathrm{B}}=\frac{1}{6}\begin{bmatrix} -1 & 3 & -3 & 1 \\ 3 & -6 & 3 & 0 \\ -3 & 0 & 3 & 0 \\ 1 & 4 & 1 & 0 \end{bmatrix}, \boldsymbol{C}_{\mathrm{CR}}=\frac{1}{2}\begin{bmatrix} -1 & 3 & -3 & 1 \\ 2 & -5 & 4 & -1 \\ -1 & 0 & 1 & 0 \\ 0 & 2 & 0 & 0 \end{bmatrix}. \tag{3}$$

Step 2: mathematical modelling of the linear filter

The output $q[n]$ of the LF (finite impulse response (FIR) filter) block, as shown in Fig. 1, is expressed as $q[n]=\boldsymbol{h}_n^{\mathrm{T}}\boldsymbol{g}_n$, where $\boldsymbol{h}_n\in\mathbb{R}^{N\times 1}=[\, h[0], h[1], ..., h(N-1)\,]^{\mathrm{T}}$ is the weight vector of the adaptive LF of length N, the signal vector is $\boldsymbol{g}_n=[\, g[n], g[n-1], ...,$

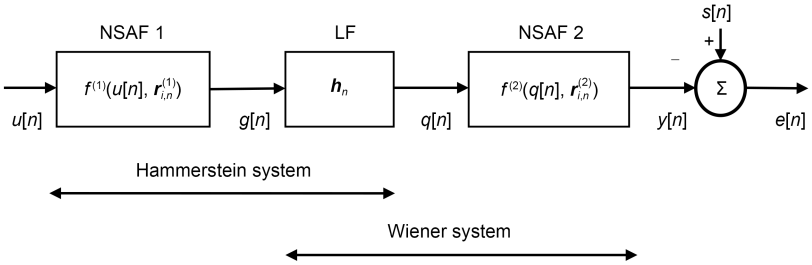

Fig. 1 Schematic of a Hammerstein–Wiener spline adaptive filter (HW-SAF) system

$g[n-N+1]]^{\mathrm{T}}$, and $g[n]$ is the output of NSAF 1, as given in Eq. (2).

Step 3: mathematical modelling of NSAF 2

The output $q[n]$ of the LF block is the input to the NSAF 2 block (Fig. 1). Like NSAF 1, the relationship between the input $q[n]$ and output $y[n]$ of NSAF 2 is expressed as $y[n]=f^{(2)}(q[n], \boldsymbol{r}_{i,n}^{(2)})$ (Scarpiniti et al., 2015b), where $f^{(2)}(\cdot)$ and $\boldsymbol{r}_{i,n}^{(2)}$ denote the nonlinear spline function and spline control point vector of NSAF 2, respectively. $\boldsymbol{r}_{i,n}^{(2)}$ is represented by $\boldsymbol{r}_{i,n}^{(2)}\in\mathbb{R}^{4\times1}=[r_{i,n}^{(2)}, r_{i+1,n}^{(2)}, r_{i+2,n}^{(2)}, r_{i+3,n}^{(2)}]^{\mathrm{T}}$. The mathematical formulae to evaluate the parameters ρ and i at time index n for NSAF 2 are as follows:

$$\begin{cases} i_n^{(2)} = \lfloor q[n]/\Delta u^{(2)} \rfloor + (R^{(2)} - 1)/2, \\ \rho_n^{(2)} = q[n]/\Delta u^{(2)} - \lfloor q[n]/\Delta u^{(2)} \rfloor. \end{cases} \tag{4}$$

The response $y[n]$ of the NSAF 2 block for the input $q[n]$ is mathematically expressed as

$$y[n] = \left(\boldsymbol{\rho}_{i,n}^{(2)}\right)^{\mathrm{T}} \boldsymbol{C}\boldsymbol{r}_{i,n}^{(2)}, \tag{5}$$

where $\boldsymbol{\rho}_{i,n}^{(2)}\in\mathbb{R}^{4\times1}=[\rho_{i,n}^{3(2)}, \rho_{i,n}^{2(2)}, \rho_{i,n}^{(2)}, 1]^{\mathrm{T}}$ and the 4×4 spline basis matrix $\boldsymbol{C}$ is given in Eq. (3). Assuming that the signal $s[n]$ is the output of an unknown system corrupted with the additive Gaussian noise (zero mean and constant variance σ^2), the error signal $e[n]$ (Fig. 1) is given by $e[n]=s[n]-y[n]$, where $y[n]$ is given in Eq. (5).

Step 4: fitness function formulation for the HW-SAF system design

In this study, the cost or fitness function J_1 of the HW-SAF system is obtained as follows:

$$J_1(\boldsymbol{h}_n, \boldsymbol{\rho}_{i,n}^{(1)}, \boldsymbol{\rho}_{i,n}^{(2)}) = \frac{1}{L}\sum_{l=1}^{L} e^2[l], \tag{6}$$

where L is the length of data samples.

A pictorial representation of the mathematical analysis of the above steps is presented in Fig. S1 in the supplementary materials for better understanding.

2.2 Mathematical modelling of WH-SAF and its cost function formulation

A schematic of WH-SAF is shown in Fig. 2, where an NSAF is sandwiched between two linear filter FIR blocks (LF 1 and LF 2) (Scarpiniti et al., 2015b). Both LF 1 and LF 2 are designed with the FIR filter. The symbols corresponding to the LF 1 and LF 2 blocks are denoted by the superscripts 1 and 2, respectively. From Fig. 2, the outputs of LF 1, NSAF, and LF 2 blocks are mathematically expressed as follows (Scarpiniti et al., 2015b):

$$g[n] = \left(\boldsymbol{h}_n^{(1)}\right)^{\mathrm{T}} \boldsymbol{u}_n = \sum_{j=0}^{N_1} h_n^{(1)}[j]\, u[n-j], \tag{7}$$

$$q[n] = f(\boldsymbol{g}[n], \boldsymbol{r}_{i,n}) = \boldsymbol{\rho}_{i,n}^{\mathrm{T}} \boldsymbol{C}\boldsymbol{r}_{i,n}, \tag{8}$$

$$y[n] = \left(\boldsymbol{h}_n^{(2)}\right)^{\mathrm{T}} \boldsymbol{q}_n = \sum_{k=0}^{N_2} h_n^{(2)}[k]\, q[n-k]. \tag{9}$$

Herein $\boldsymbol{h}_n^{(1)}\in\mathbb{R}^{N_1\times1}=[h_n^{(1)}[n], h_n^{(1)}[n-1], ..., h_n^{(1)}[n-N_1+1]]^{\mathrm{T}}$ and $\boldsymbol{h}_n^{(2)}\in\mathbb{R}^{N_2\times1}=[h_n^{(2)}[n], h_n^{(2)}[n-1], ..., h_n^{(2)}[n-N_2+1]]^{\mathrm{T}}$ are the coefficient vectors of LF 1 and LF 2, respectively; $\boldsymbol{u}_n\in\mathbb{R}^{N_1\times1}=[u[n], u[n-1], ..., u[n-N_1+1]]^{\mathrm{T}}$ is the input signal vector; parameter $\boldsymbol{q}_n\in\mathbb{R}^{N_2\times1}=[q[n], q[n-1], ..., q[n-N_2+1]]^{\mathrm{T}}$; local spline parameter $\boldsymbol{\rho}_{i,n}\in\mathbb{R}^{4\times1}=[\rho_{i,n}^3, \rho_{i,n}^2, \rho_{i,n}, 1]^{\mathrm{T}}$; spline control point vector $\boldsymbol{r}_{i,n}\in\mathbb{R}^{4\times1}=[r_{i,n}, r_{i+1,n}, r_{i+2,n}, r_{i+3,n}]^{\mathrm{T}}$ and 4×4 spline basis matrix $\boldsymbol{C}$ are given in Eq. (3). The symbols N_1 and N_2 denote the lengths of the filter coefficients of LF 1 and LF 2, respectively. The error signal $e[n]$ (Fig. 2) is given by $e[n]=s[n]-y[n]$, where $y[n]$ is given in Eq. (9). The cost function J_2 for the WH-SAF system is defined in Eq. (10):

$$J_2(\boldsymbol{h}_n^{(1)}, \boldsymbol{h}_n^{(2)}, \boldsymbol{r}_{i,n}) = \frac{1}{L}\sum_{l=1}^{L} e^2[l]. \tag{10}$$

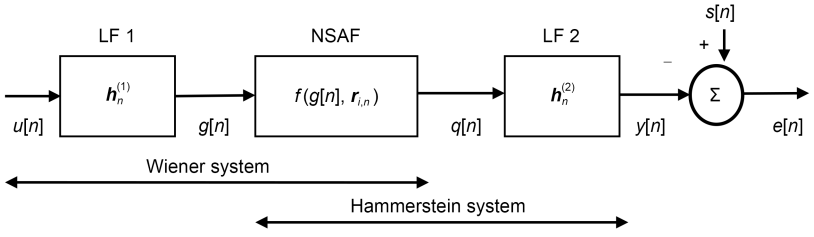

Fig. 2 Schematic of a Wiener–Hammerstein spline adaptive filter (WH-SAF) system

In this study, the main aim of using MOA (i.e., ROA) is to minimise the cost function J_1 or J_2 by jointly adapting the linear filter and spline control point weights. If J_1 or J_2 tends to zero, then the response of CSAF closely meets the actual output.

3 Proposed ROA-based CSAF design for unknown system modelling

MOAs are efficient in solving very complex problems (Janjanam et al., 2022d, 2023; Yan et al., 2023). Hence, in this study, various well-established MOAs such as ROA (Jia HM et al., 2021), MVO (Mirjalili et al., 2016), BSO (Shi, 2011), and DE (Storn and Price, 1997) are individually applied to solve the parameter estimation problem of recently introduced CSAFs. Due to page constraints, we do not explain the basics and functional steps of MVO, BSO, and DE algorithms. Researchers may refer to Mirjalili et al. (2016), Shi (2011), and Storn and Price (1997) for these algorithms. However, we present the step-by-step procedure of the ROA method for the design of CSAFs.

ROA (Jia HM et al., 2021) is a recently matured bio-inspired MOA that works on the principle of the parasitic behaviour and the random host replacement strategy of remora fish. The basic elementary details of ROA can be found in Jia HM et al. (2021). In ROA, the remora commonly follows the optimisation strategies of both humpback whales and swordfish. Hence, ROA has the benefits of both the whale optimisation algorithm (WOA) (Mirjalili and Lewis, 2016) and sailfish optimisation algorithm (SFO) (Shadravan et al., 2019) when dealing with optimisation problems.

To obtain optimal solutions, ROA adopts the exploration (global search) and exploitation (local search) process by using the "free travel" and "eat thoughtfully" techniques, respectively. To perform the free travel operation, ROA uses the methods of SFO and experiment attack. The WOA strategy and host feeding strategies are used to conduct the eating thoughtfully technique. The mathematical analysis to describe the position updating rules for this strategy was established by Jia HM et al. (2021) and is used in this study for the optimisation of cost functions, as given in Eqs. (6) and (10).

The mechanism to design a CSAF for an unknown plant estimation using ROA proceeds mainly by the initialisation of search agents, fitness function evaluation for each search agent, and exploitation and exploration phases, which are discussed in detail below. The respective flowchart and pseudocode are shown in Fig. 3 and Table S1 in the supplementary materials, respectively.

Step 1: initialise the problem design variables (WH-SAF or HW-SAF parameters) in the search space

Randomly develop NP, the number of search agents, where the position of each search agent is designated with the variables of the problem. The search space of each agent is filled with the parameters required to be optimised, such as spline control points $\boldsymbol{r}_n$ and linear filter coefficients $\boldsymbol{h}_n$. Moreover, randomly designate each parameter using

$$\begin{aligned} B_k^j &= \mathrm{lb} + \mathrm{rand}\,(0, 1) \cdot (\mathrm{ub} - \mathrm{lb}), \\ k &= 1, 2, ..., \mathrm{NP},\ j = 1, 2, ..., \varpi, \end{aligned} \tag{11}$$

where rand(0, 1) produces the random values between 0 and 1, and the lower and upper boundaries of each parameter are represented by lb and ub, respectively. The vector representations of each agent (remora) for the HW-SAF and WH-SAF problems are given in Eqs. (12) and (13), respectively. Moreover, the dimension of each agent is $1 \times \varpi$, where ϖ denotes the total number of parameters. Therefore, the total dimension is $\mathrm{NP} \times \varpi$.

$$\begin{aligned} \boldsymbol{B}_{\mathrm{H}} = [\, & h[0], h[1], ..., h(N-1), \\ & r_1^{(1)}, r_2^{(1)}, ..., r_R^{(1)}, r_1^{(2)}, r_2^{(2)}, ..., r_R^{(2)}\,], \end{aligned} \tag{12}$$

$$\begin{aligned} \boldsymbol{B}_{\mathrm{W}} = [\, & h^{(1)}[0], h^{(1)}[1], ..., h^{(1)}[n - N_1], h^{(2)}[0], \\ & h^{(2)}[1], ..., h^{(2)}[n - N_2], r_1, r_2, ..., r_R\,]. \end{aligned} \tag{13}$$

Step 2: evaluate the fitness of each remora

Determine the fitness values for all the agents' positions using the fitness function J_1 or J_2 as given in Eqs. (6) and (10), and then store the lowest error fitness value for the corresponding position (best) in B_{best}.

Step 3: determine the values of algorithm-specific parameters in each iteration

Amend the parameters β, γ, and ξ using the following equations:

$$\beta = \mathrm{rand}\,(0, 1) \cdot (\gamma - 1) + 1, \tag{14}$$

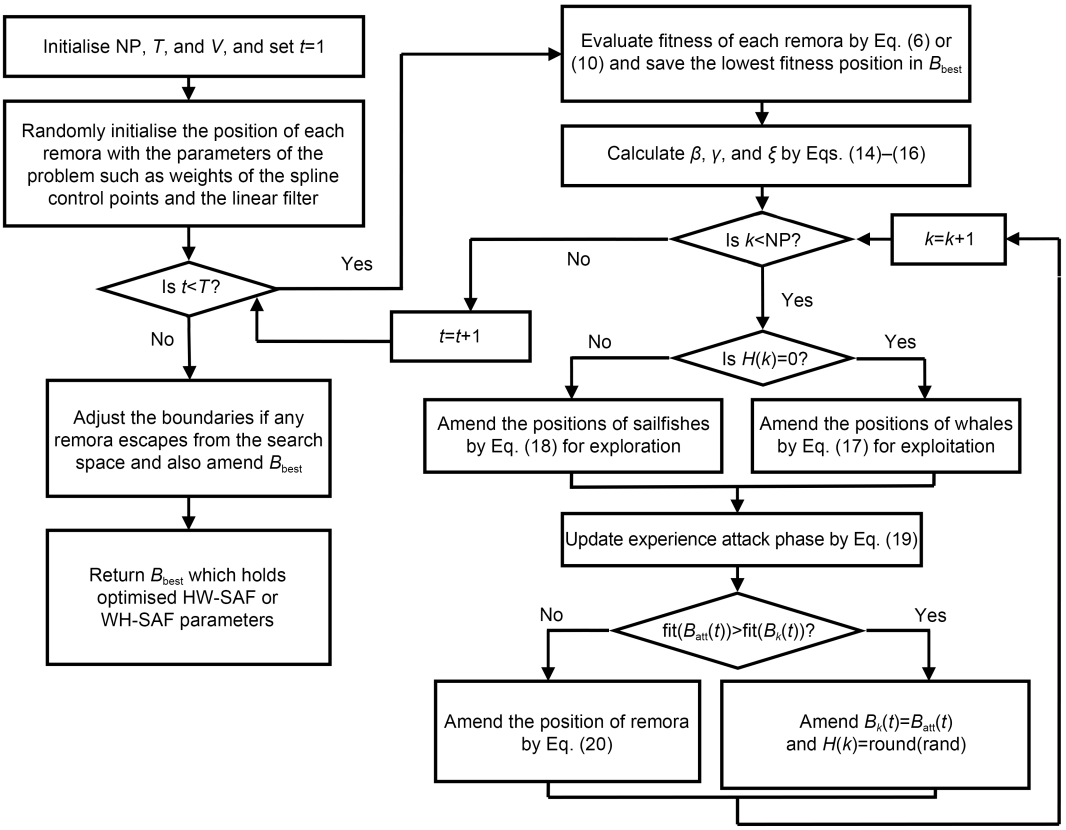

Fig. 3 Flowchart of cascaded spline adaptive filter (CSAF) system identification using the remora optimisation algorithm (ROA) method

$$\gamma = -(1 + t/T), \tag{15}$$

$$\xi = 2(1 - t/T), \tag{16}$$

where t is the current epoch number, T is the maximum epoch number, β takes random values in [−1, 1], and γ goes down linearly in [−2, −1].

Step 4: perform exploitation and exploration mechanisms for each search agent

Repeat steps 1 and 2 for each search agent, k= 1, 2, ..., NP.

(1) If the selection parameter $H(k)$=0, then perform the eat thoughtfully method to achieve good exploitation (Jia HM et al., 2021). In this method, the positions of the attached whales are updated using Eq. (17); otherwise, execute step 6.

$$B_k(t+1) = D\mathrm{e}^{\beta}\cos(2\pi\beta) + B_k(t), \tag{17}$$

where $B_k(t)$ is the current position, β is a random value in [−1, 1] as given in Eq. (14), and D is the distance between the best and the current positions, $D = \left| B_{\text{best}}(t) - B_k(t) \right|$.

(2) If $H(k)$=1, then carry out the free travel method for exploration, where the positions of the attached sailfishes are updated using Eq. (18):

$$B_k(t+1) = B_{\text{best}}(t) - \left(\text{rand}(0,1) \cdot \frac{B_{\text{best}}(t) + B_{\text{rand}}(t)}{2} - B_{\text{rand}}(t) \right), \tag{18}$$

where $B_{\text{rand}}(t)$ is a random position.

(3) Construct a one-step prediction through experience attack. In this activity, the remora makes continuous small steps around the host to decide whether it is required to replace the host. This mechanism is given in Eq. (19) (Jia HM et al., 2021):

$$B_{\text{att}}(t+1) = B_k(t) + \text{rand} \cdot (B_k(t) - B_{\text{pre}}(t)), \tag{19}$$

where rand denotes the random small global step, and $B_{\text{pre}}(t)$ and $B_{\text{att}}(t)$ represent the previous generation's location and the location of the tentative step, respectively.

(4) If the fitness value of the attempted response $\text{fit}(B_{\text{att}}(t))$ is greater than the fitness value of the current response, $\text{fit}(B_k(t))$ then amends the position of remora $B_k(t)$ with $B_{\text{att}}(t)$ and sets $H(k)$=round(rand). Conversely, if $\text{fit}(B_{\text{att}}(t))<\text{fit}(B_k(t))$, then the remora chooses the host feeding phase for local optimisation. In this phase, the position of the remora is updated by the following (Jia HM et al., 2021):

$$\begin{cases} B_k(t+1) = B_k(t+1) + F, \\ F = G(B_k(t) - VB_{\text{best}}(t)), \end{cases} \tag{20}$$

where

$$G = 2\xi \cdot \text{rand}(0, 1) - \xi, \tag{21}$$

and F denotes the small step change of the remora position, which corresponds to the volume space of the remora and host. To show the deviation between the positions of the remora and the host, the remora factor V is used to narrow down the location of the remora. ξ is defined in Eq. (16).

Step 5: confinement process

Update the boundaries (lb and ub) if any agent escapes from the problem search space boundary. Update the position B_{best}.

Step 6: termination criterion for the ROA algorithm

Repeat steps 2 to 5 until the stopping condition is reached and then declare that B_{best} carries globally optimised HW-SAF or WH-SAF system parameters.

4 Simulation results and analysis

In this section we present MATLAB software based simulation results to demonstrate the effectiveness of the proposed ROA-based design technique for three numerical and two real-time systems. The first and second numerical systems have the HW-SAF and WH-SAF architectures, respectively, while the third system has an HW architecture. Moreover, we applied the respective architecture type to design the first and second systems. However, the third numerical system was identified using numerous well-known models. To substantiate the efficacy of the ROA-based design approach, three MOAs, namely MVO, BSO, and DE techniques, were independently applied to the same problem, and the various performance metrics obtained were compared. The numerical values of the MOAs' control parameters vary based on the problem. Hence, we simulated each algorithm multiple times and chose the best set of control parameter values. We used the strategy described by Janjanam et al. (2022a) and Nayak et al. (2019) to fix the values of the lower bound (lb) and upper bound (ub) of the problem design variables, the number of populations (NP), and the maximum number of iterations (T). The selected lb, ub, NP, and T values were −10, 10, 25, and 1000, respectively. The justification for choosing these common control parameter values for all algorithms is provided in the supplementary materials. The other algorithm-specific parameter values, selected after performing exhaustive experiments and based on the knowledge from the literature (Storn and Price, 1997; Shi, 2011; Mirjalili et al., 2016; Jia HM et al., 2021), were as follows: (1) crossover rate=0.8 and scaling factor=0.4 for DE; (2) slope of logarithmic sigmoid function=25 and predefined probabilities p_1=0.3, p_2=0.7, p_3=0.5, and p_4=0.4 for BSO; (3) contrast parameter=0.5, mining capability=1/6, random parameter∈[0, 1], wormhole existence probability∈[0.3, 1], and travelling distance rate∈[0, 1] for MVO; (4) remora factor V=0.5 for ROA.

For a fair comparison, all algorithms were simulated on the same platform (64-bit Windows 7, Intel i5 CPU, 3.20 GHz processor, and 4 GB RAM). Moreover, 1100 random input data samples (∈[−1, 1]) were generated. The first 1000 samples were allotted for the identification (estimation) process, and the remaining 100 for the validation (testing) process.

4.1 Identification of unknown systems 1 and 2

The mathematical forms of unknown nonlinear systems 1 and 2 are presented below and were identified in the same form as in the estimation model.

System 1: system 1 (Scarpiniti et al., 2015b) is of WH-SAF architecture (Fig. 2). The coefficients of LF 1 and LF 2 blocks are presented mathematically in Eqs. (22) and (23), respectively. In comparison, the nonlinear function of the NSAF block was modelled with the 23-point LUT having the control point vector $\boldsymbol{r}_n$ defined in Eq. (24) and Δu=0.2 (Scarpiniti et al., 2015b).

$$\text{LF 1: } \boldsymbol{h}_n^{(1)}=[\,0.6,\,-0.4,\,0.25,\,0.1,\,-0.05,\,0.001\,]^{\mathrm{T}}, \tag{22}$$

$$\text{LF 2: } \boldsymbol{h}_n^{(2)}=[\,1,\,0.5,\,-0.25,\,0.15,\,0.25,\,-0.10,\,0.05\,]^{\mathrm{T}}, \tag{23}$$

$$\begin{aligned}\text{NSAF: } \boldsymbol{r}_n=[&-2.2,\,-2.0,\,-1.8,\,...,\,-1.0,\,-0.8,\,-0.91,\\ &-0.40,\,-0.20,\,...,\,0.05,\,0.0,\,-0.40,\\ &0.58,\,1.0,\,1.0,\,1.2,\,1.4,\,...,\,2.2\,]^{\mathrm{T}}.\end{aligned} \tag{24}$$

System 2: system 2 (Scarpiniti et al., 2015b) is of HW-SAF architecture (Fig. 1). The internal blocks of HW-SAF structure, such as LF, NSAF 1, and NSAF 2, are mathematically described in Eqs. (25)–(27), where the nonlinear functions of the two NSAF blocks are modelled with the 23-point LUT having the control points $\boldsymbol{r}_n^{(1)}$ and $\boldsymbol{r}_n^{(2)}$. Moreover, the spacing between the samples is Δu=0.2 (Scarpiniti et al., 2015b).

$$\text{LF: } \boldsymbol{h}_n=[\,0.6,\,-0.4,\,0.25,\,0.1,\,-0.05,\,0.001\,]^{\mathrm{T}}, \tag{25}$$

$$\begin{aligned}\text{NSAF 1: } \boldsymbol{r}_n^{(1)}=[&-2.2,\,-2.0,\,-1.8,\,...,\,-1.0,\,-0.8,\,-0.91,\\ &-0.40,\,...,\,-0.20,\,0.05,\,0.0,\,-0.40,\,0.58,\\ &1.0,\,1.0,\,1.2,\,1.4,\,...,\,2.2\,]^{\mathrm{T}},\end{aligned} \tag{26}$$

$$\begin{aligned}\text{NSAF 2: } \boldsymbol{r}_n^{(2)}=[&-2.2,\,-2.0,\,-1.8,\,...,\,-1.0,\,-0.8,\\ &-0.60,\,-0.10,\,...,\,-0.20,\,0.0,\,0.02,\,0.40,\\ &0.60,\,0.8,\,1.35,\,1.2,\,1.4,\,...,\,2.2\,]^{\mathrm{T}}.\end{aligned} \tag{27}$$

4.1.1 Parameter convergence profiles

The best run convergence characteristics (out of 100 independent runs) for system 1 (WH-SAF) and system 2 (HW-SAF) using the proposed ROA-based design technique (at noise variance σ^2=0.001^2) are graphically illustrated in Fig. 4 and Fig. S2 in the supplementary materials, respectively. The spline control point vectors of each NSAF block of each system carried 23 coefficients (Eqs. (24), (26), and (27)). However, due to space constraint, we present convergence profiles only for the most important coefficients of the control point vector (Figs. 4, S2b, and S2c), as recommended by Scarpiniti et al. (2013). Figs. 4 and S2 show that the linear filter FIR coefficients of both systems converged to their optimum values at about 580 iterations, and that the NSAF control points took around 650 iterations. In addition, Fig. 4 shows that the achieved optimal values closely matched the true values. The various metrics (Mehmood et al., 2019a) such as MAE, RMSD, MWD, and TIC results are presented in Table 1.

The absolute error AE=$\left|\varphi_m-\hat{\varphi}_m\right|$ (Mehmood et al., 2019b) was used to measure the deviation between the achieved optimal estimated coefficient $\hat{\varphi}$ and the true coefficient φ. The values obtained for systems 1 and 2 using ROA, MVO, BSO, and DE algorithms under three noise variance levels (σ^2=0.001^2, 0.01^2, and 0.1^2) are graphically presented in Fig. 5 and Fig. S3 in the supplementary materials, respectively. The graphs are shown on a semi-logarithmic scale to increase the visibility. Fig. 5 shows that AE values of system 1 for the noise level σ^2 equal to 0.001^2, 0.01^2, and 0.1^2 lay in the ranges of 10^{-9} to 10^{-7} , 10^{-7} to 10^{-5}, and 10^{-5} to 10^{-4}, respectively, using ROA, 10^{-8} to 10^{-7}, close to 10^{-6}, and close to10^{-4}, respectively, using MVO, 10^{-7}

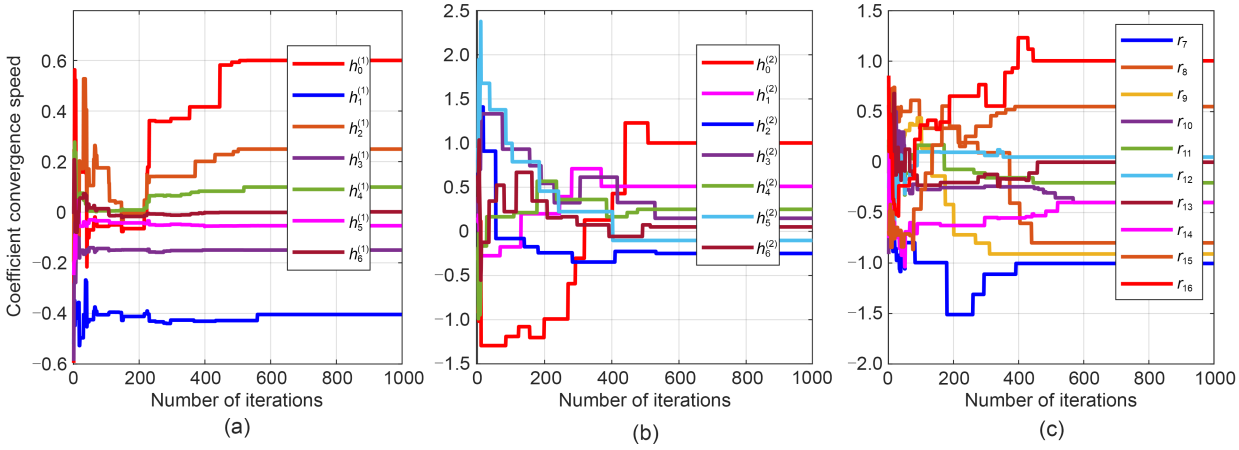

Fig. 4 Parameter convergence profiles of system 1 for the best run of the ROA technique: (a) FIR filter 1; (b) FIR filter 2; (c) control points of NSAF (References to colour refer to the online version of this figure)

Table 1 Comparison of various performance indices for the techniques used for system 1

Method	σ^2	MAE	RMSD	MWD	TIC	Fitness (J_1/J_2)	CT (s)	$\text{Number}_{\text{best}}$
ROA	0.001^2	9.54E-09	1.76E-09	1.39E-08	3.21E-08	2.75E-14	0.432	509
	0.01^2	4.33E-08	8.92E-08	3.66E-07	4.56E-07	2.77E-10	0.424	424
	0.1^2	2.99E-06	3.11E-07	3.51E-06	1.76E-05	6.44E-09	0.437	280
MVO	0.001^2	8.55E-08	6.54E-08	5.55E-07	3.65E-07	3.76E-12	0.625	553
	0.01^2	7.45E-06	7.43E-06	6.87E-06	4.87E-06	7.11E-10	0.620	435
	0.1^2	1.23E-05	5.98E-05	4.23E-04	1.67E-05	4.65E-08	0.617	289
BSO	0.001^2	5.66E-07	4.76E-07	6.31E-05	3.89E-06	2.87E-09	0.901	569
	0.01^2	3.33E-06	4.54E-05	8.55E-04	2.54E-05	1.65E-08	0.893	484
	0.1^2	6.12E-04	6.36E-04	7.42E-03	1.43E-04	4.28E-07	0.899	328
DE	0.001^2	1.98E-05	5.21E-04	3.37E-04	3.72E-03	3.65E-07	0.943	407
	0.01^2	3.22E-03	2.43E-03	8.22E-03	2.22E-02	2.83E-05	0.947	385
	0.1^2	2.43E-02	8.21E-03	3.54E-02	7.89E-02	3.47E-03	0.940	257

$\text{Number}_{\text{best}}$: the number of iterations of the best fitness

to 10^{-6}, 10^{-6} to 10^{-5}, and close to 10^{-4} , respectively, using BSO, and 10^{-5} to 10^{-4}, 10^{-5} to 10^{-4}, and 10^{-3} to 10^{-1}, respectively, using DE. From Fig. S3, the magnitudes of AE metric values of system 2 for the noise variances σ^2 equal to 0.001^2, 0.01^2, and 0.1^2 lay in the ranges of 10^{-7} to 10^{-6}, 10^{-6} to 10^{-4}, and 10^{-4} to 10^{-2}, respectively, using ROA, 10^{-6} to 10^{-4}, 10^{-5} to 10^{-3}, and 10^{-3} to 10^{-2}, respectively, using MVO, 10^{-5} to 10^{-4}, 10^{-4} to 10^{-3}, and 10^{-3} to 10^{-2}, respectively, using BSO, and 10^{-3} to 10^{-2}, 10^{-2} to 10^{-1}, and 10^{-1} to 10^{0}, respectively, using DE.

From the above results, we have drawn the following conclusions: (1) the performance of each chosen MOA decreased with the rise in the noise level, (2) significantly lower values were achieved by using the ROA-based identification approach compared to others, and (3) marginally superior AE results were achieved for system 1 (WH-SAF) than for system 2 (HW-SAF) using the MOAs because system 1 had lower nonlinearity. Furthermore, the fitness functions (Eqs. (6) and (10)) were measured using the estimated coefficients obtained in the best simulation run.

The fitness values secured in each iteration for systems 1 and 2 modelling using the presented algorithms under different noise levels are shown in Fig. 6 and Fig. S4 in the supplementary materials, respectively, and the reported optimum fitness values in Table 1 and Table S2 in the supplementery materials. Tables 1 and S2 also show the iteration number corresponding to the best fitness value and the computation time (CT) required by the chosen algorithm to complete 1000 iterations for systems 1 and 2.

It is clear from Fig. 6 that for the three noise variance levels $\sigma^2=0.001^2$, 0.01^2, and 0.1^2, the case of system 1 modelling gave the optimum fitness order of 10^{-14}, 10^{-10}, and 10^{-9}, respectively, after completion of 509, 424, and 280 iterations by the ROA-based approach, 10^{-12}, 10^{-10}, and 10^{-8}, respectively, after 553, 435, and 289 iterations using the MVO method, 10^{-9}, 10^{-8}, and 10^{-7}, respectively, after 569, 484, and 328 iterations using the BSO method, and 10^{-7}, 10^{-5}, and 10^{-3}, respectively, after 407, 385, and 257 iterations using the DE method.

An analytical description of the fitness convergence profile for system 2 is provided in the supplementary materials. The convergence speed of the presented techniques was ordered: DE>ROA>MVO>BSO. The improvement of the proposed ROA-based design technique over other chosen algorithms for systems 1 and 2 in terms of different metrics under the noise variance level $\sigma^2=0.001^2$ is shown in Fig. S5 in the supplementary materials. The improvement achieved using ROA over MVO, BSO, and DE for systems 1 and 2 for the metrics lay in the ranges of 88.84% to 99.99% and 76.89% to 99.99%, respectively.

4.1.2 Robustness performance analysis

In general, the performance of MOAs varies in each run (Jia HM et al., 2021). Hence, the robustness of the MOAs used for systems 1 and 2 was examined

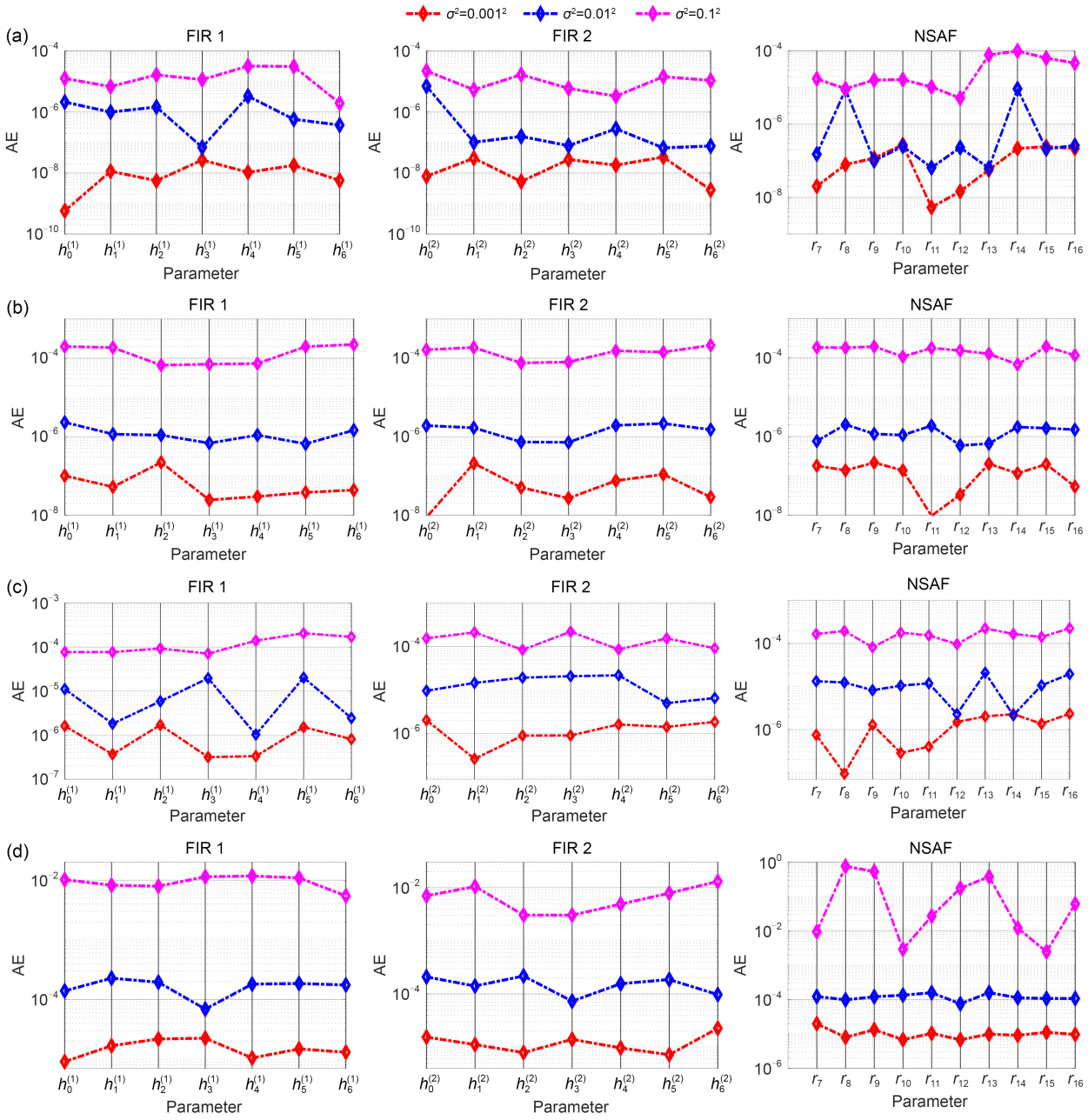

Fig. 5 AE metric results for system 1 by the ROA (a), MVO (b), BSO (c), and DE (d) algorithms under different noise levels

by simulating each algorithm in 100 independent runs. The statistics (best, worst, and mean) of the estimated coefficients of systems 1 and 2 obtained using the chosen algorithms under the noise level σ^2=0.001^2 are listed in Table 2 and Table S3 in the supplementary materials, respectively.

Tables 2 and S3 show that the statistical results achieved through the ROA method were closer to the actual coefficients than those of other schemes. Moreover, there was no noticeable deviation between the results of the ROA and MVO techniques. However, both techniques outperformed the BSO and DE methods. Tables 2 and S3 also show that the mean results (average of 100 runs) of the ROA and DE schemes almost equaled the best run results. Furthermore, the robustness of the MOAs used is demonstrated through the global metrics such as the global mean absolute error (GMAE), global root mean square deviation (GRMSD), global Thiel's inequality coefficient (GTIC), and global fitness (GFIT) (Mehmood et al.,

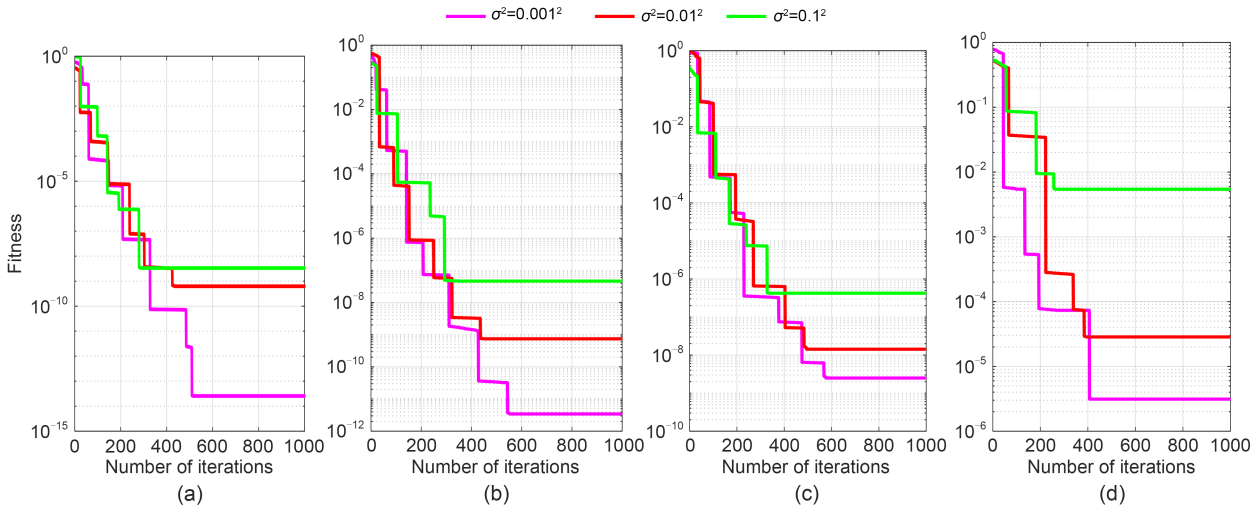

Fig. 6 Fitness convergence profiles for system 1 using the ROA (a), MVO (b), BSO (c), and DE (d) algorithms under different noise levels

2019a). Each metric was measured using the estimation results of 100 independent simulation runs. The attained mean and standard deviation (STD) values corresponding to each metric for systems 1 and 2 under different noise scenarios (σ^2=0.001^2, 0.01^2, and 0.1^2) are given in Table 3 and Table S4 in the supplementary materials, respectively.

For systems 1 and 2, Tables 3 and S4 show that the mean values of the GFIT metric were around 10^{-14} to 10^{-7} for ROA, 10^{-13} to 10^{-8} for MVO, 10^{-9} to 10^{-5} for BSO, and 10^{-7} to 10^{-3} for DE. The ranges of magnitude levels for other global metrics, namely GMAE, GRMSD, and GTIC, were from about 10^{-9} to 10^{-4} for ROA, 10^{-8} to 10^{-3} for MVO, 10^{-6} to 10^{-3} for BSO, and 10^{-5} to 10^{-1} for DE. Moreover, Tables 3 and S4 show that the mean values of all the global metrics corresponding to the ROA and DE algorithms were nearer to the best-run results (Table 1). Furthermore, the STD values of all the metrics corresponding to the ROA method (with the noise level σ^2=0.001^2) were closer to zero (from 10^{-14} to 10^{-9}) than those of the competing approaches.

Further, the fitness metric results on 100 independent runs of the ROA, MVO, BSO, and DE algorithms for systems 1 and 2 under various noise scenarios are graphically presented in Fig. 7 and Fig. S6 in the supplementary materials, respectively. Figs. 7 and S6 show that the MVO and BSO algorithms showed substantial fluctuations. At the same time, DE and the proposed ROA-based methods exhibited little volatility. However, DE showed poor results. Thus, the independent test indicates that the proposed ROA-based approach shows better robust performance and the performance is statistically significantly better than those of others. Additionally, the consistency of ROA over the MVO, BSO, and DE algorithms for the design of CSAFs (systems 1 and 2) was verified using Holm's test (Holm, 1979; Shadravan et al., 2019; Braik et al., 2022). The procedure for conducting Holm's test and results (Table S5) obtained for both systems are provided in the supplementary materials.

4.1.3 Computational complexity analysis

Generally, a particular technique's CC is denoted by notation O. CC of the algorithms used for the chosen system 1 (HW-SAF) and system 2 (WH-SAF) was calculated based on the literature (Jia HM et al., 2021; Janjanam et al., 2022a; Yadav et al., 2023). CC of MOA is $O(\text{MOA})=O(F(x))O(\text{NP}\cdot(T\varpi+1))$ (refer to the supplementary materials for proof), where $F(x)$ denotes the fitness function of the chosen problem, NP is the population size, T is the maximum iteration number, and ϖ is the dimension of the problem.

In this study, CC of the algorithms used for modelling systems 1 and 2 was also examined with the help of runtime. Consider T_0=CT/T×NP, T_1=CT/T, and T_2=average time of K independent runs, where CT denotes the computational time taken by the algorithm for one iteration (Janjanam et al., 2022a; Yadav et al.,

Table 2 Statistical results of the estimated parameters of system 1 using chosen algorithms under the noisy condition $\sigma^2=0.001^2$

Method	Metric	FIR filter 1			FIR filter 2			NSAF			
ROA	Best	0.600	−0.150	0.001	0.999	0.150	0.049	−1.000	−0.401	0.000	0.999
		−0.401	0.101	N/A	0.498	0.248	N/A	−0.798	−0.199	−0.402	N/A
		0.249	−0.050	N/A	−0.249	−0.101	N/A	−0.900	0.049	0.579	N/A
	Mean	0.601	−0.149	0.001	1.020	0.150	0.050	−1.001	−0.401	0.000	1.001
		−0.400	0.100	N/A	0.499	0.248	N/A	−0.799	−0.199	−0.402	N/A
		0.249	−0.049	N/A	−0.248	−0.100	N/A	−0.909	0.050	0.578	N/A
	Worst	0.598	−0.149	0.001	1.000	0.150	0.049	−0.098	−0.398	0.000	0.998
		−0.401	0.009	N/A	0.497	0.248	N/A	−0.798	−0.199	−0.401	N/A
		0.249	−0.049	N/A	−0.246	−0.095	N/A	−0.908	0.049	0.577	N/A
MVO	Best	0.589	−0.142	0.0009	0.961	0.141	0.042	−0.992	−0.396	0.001	0.989
		−0.388	0.093	N/A	0.445	0.239	N/A	−0.785	−0.192	−0.389	N/A
		0.240	−0.045	N/A	−0.234	−0.092	N/A	−0.892	0.048	0.571	N/A
	Mean	0.589	−0.143	0.0009	0.960	0.141	0.043	−0.993	−0.397	0.001	0.991
		−0.389	0.091	N/A	0.444	0.240	N/A	−0.786	−0.194	−0.390	N/A
		0.242	−0.044	N/A	−0.235	−0.091	N/A	−0.892	0.048	0.573	N/A
	Worst	0.588	−0.141	0.0009	0.959	0.140	0.040	−0.991	−0.395	0.001	0.988
		−0.387	0.090	N/A	0.443	0.240	N/A	−0.783	−0.194	−0.390	N/A
		0.240	−0.045	N/A	−0.235	−0.091	N/A	−0.890	0.048	0.570	N/A
BSO	Best	0.521	−0.132	0.0008	0.911	0.135	0.035	−0.936	−0.380	0.002	0.935
		−0.312	0.083	N/A	0.398	0.226	N/A	−0.716	−0.132	−0.329	N/A
		0.211	−0.038	N/A	−0.204	−0.083	N/A	−0.825	0.033	0.523	N/A
	Mean	0.520	−0.133	0.0008	0.910	0.134	0.035	−0.938	−0.381	0.002	0.936
		−0.313	0.085	N/A	0.399	0.227	N/A	−0.715	−0.135	−0.330	N/A
		0.213	−0.038	N/A	−0.205	−0.084	N/A	−0.827	0.033	0.525	N/A
	Worst	0.519	−0.133	0.0008	0.909	0.134	0.034	−0.934	−0.380	0.002	0.933
		−0.311	0.084	N/A	0.397	0.225	N/A	−0.712	−0.136	−0.330	N/A
		0.212	−0.039	N/A	−0.203	−0.082	N/A	−0.824	0.035	0.525	N/A
DE	Best	0.476	−0.124	0.0007	0.867	0.125	0.026	−0.889	−0.301	0.003	0.887
		−0.289	0.068	N/A	0.340	0.201	N/A	−0.701	−0.121	−0.301	N/A
		0.195	−0.033	N/A	−0.190	−0.072	N/A	−0.789	0.028	0.496	N/A
	Mean	0.477	−0.124	0.0007	0.866	0.124	0.025	−0.890	−0.302	0.003	0.889
		−0.290	0.069	N/A	0.342	0.202	N/A	−0.700	−0.123	−0.300	N/A
		0.194	−0.034	N/A	−0.192	−0.075	N/A	−0.788	0.029	0.498	N/A
	Worst	0.439	−0.126	0.0005	0.855	0.116	0.019	−0.857	−0.289	0.003	0.837
		−0.285	0.062	N/A	0.333	0.190	N/A	−0.695	−0.111	−0.289	N/A
		0.190	−0.031	N/A	−0.185	−0.067	N/A	−0.739	0.022	0.466	N/A

FIR fitter 1				FIR fitter 2				NSAF			
$h_0^{(1)}$	0.6	$h_4^{(1)}$	0.1	$h_0^{(2)}$	1.0	$h_4^{(2)}$	0.25	r_7	−1.0	r_{12}	0.05
$h_1^{(1)}$	−0.4	$h_5^{(1)}$	−0.05	$h_1^{(2)}$	0.5	$h_5^{(2)}$	−0.10	r_8	−0.8	r_{13}	0.0
$h_2^{(1)}$	0.25	$h_6^{(1)}$	0.001	$h_2^{(2)}$	−0.25	$h_6^{(2)}$	0.05	r_9	−0.91	r_{14}	−0.40
$h_3^{(1)}$	−0.15			$h_3^{(2)}$	0.15			r_{10}	−0.40	r_{15}	0.58
								r_{11}	−0.20	r_{16}	1.0

N/A: not applicable

Table 3 Statistical analysis of the global metric results for system 1 using chosen algorithms under different noise levels

Method	σ^2	GMAE		GRMSD		GTIC		GFIT	
		Mean	STD	Mean	STD	Mean	STD	Mean	STD
ROA	0.001^2	8.54E-09	2.21E-09	2.55E-09	2.55E-10	7.69E-08	5.32E-11	4.09E-14	1.33E-14
	0.01^2	5.98E-08	4.33E-07	7.21E-08	4.37E-08	2.13E-07	4.47E-09	5.54E-10	5.92E-13
	0.1^2	6.65E-06	5.47E-06	3.79E-07	3.66E-07	4.25E-05	6.23E-07	7.61E-09	4.71E-11
MVO	0.001^2	3.22E-07	4.56E-08	3.76E-08	2.55E-07	5.78E-08	5.98E-10	7.50E-13	1.06E-12
	0.01^2	3.12E-06	4.89E-06	1.98E-06	4.69E-06	3.69E-06	4.47E-08	8.35E-11	5.57E-10
	0.1^2	6.79E-04	3.97E-05	2.70E-05	2.96E-04	2.87E-05	3.78E-07	9.51E-09	1.95E-09
BSO	0.001^2	1.87E-05	3.76E-09	7.32E-06	3.87E-08	7.58E-06	5.67E-12	7.53E-09	2.28E-10
	0.01^2	5.38E-04	6.43E-05	4.38E-05	5.93E-05	6.75E-05	2.59E-08	1.39E-07	9.38E-07
	0.1^2	5.77E-03	4.57E-04	1.89E-03	3.58E-04	5.91E-04	3.85E-06	5.24E-05	6.33E-06
DE	0.001^2	7.93E-05	7.85E-04	2.78E-04	4.66E-06	2.66E-03	4.69E-04	2.57E-07	4.57E-08
	0.01^2	5.33E-03	5.37E-03	3.97E-03	9.88E-03	4.58E-02	7.56E-03	5.06E-05	5.24E-06
	0.1^2	6.68E-02	3.78E-03	7.74E-03	5.23E-02	8.29E-02	4.42E-02	3.95E-03	7.09E-03

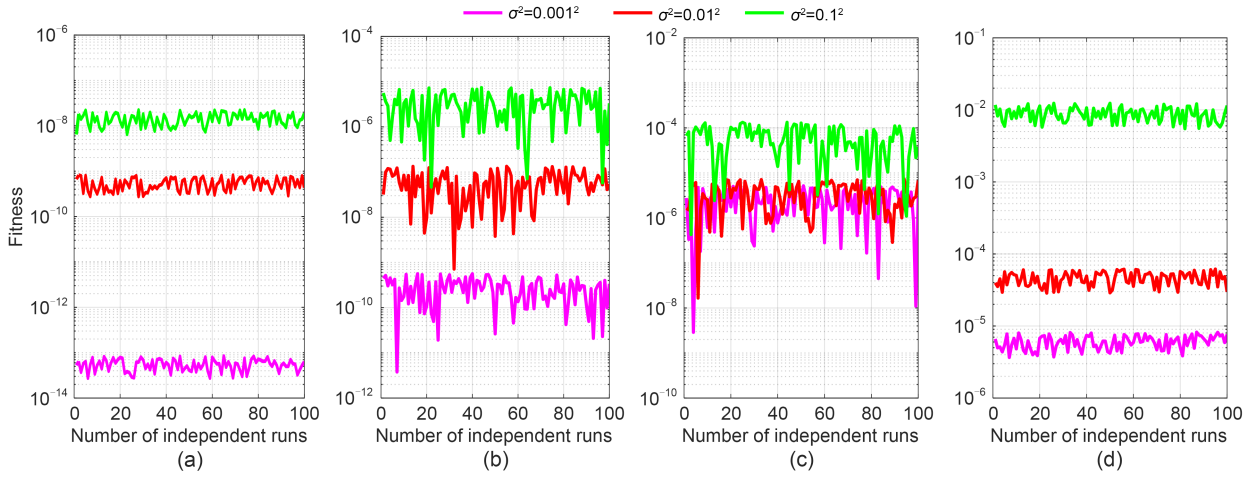

Fig. 7 Independent run results of the fitness metric for system 1 using the considered algorithms at various noise levels: (a) ROA; (b) MVO; (c) BSO; (d) DE (References to colour refer to the online version of this figure)

Table 4 Computational complexity (CC) and runtime results of systems 1 and 2 using the chosen algorithms

System	Algorithm	T_0 (s)	T_1 (s)	T_2 (s)	CC
1	ROA	1.732E-05	4.32E-04	0.426	$O(F(x))O(\mathrm{NP}\cdot(T\varpi+1))$
	MVO	2.500E-05	6.25E-04	0.618	$O(F(x))O(\mathrm{NP}\cdot(T\varpi+1))$
	BSO	3.604E-05	9.07E-04	0.893	$O(F(x))O(\mathrm{NP}\cdot(T\varpi+1))$
	DE	3.772E-05	9.43E-04	0.940	$O(F(x))O(\mathrm{NP}\cdot(T\varpi+1))$
2	ROA	2.244E-05	5.61E-04	0.554	$O(F(x))O(\mathrm{NP}\cdot(T\varpi+1))$
	MVO	2.932E-05	7.33E-04	0.728	$O(F(x))O(\mathrm{NP}\cdot(T\varpi+1))$
	BSO	3.948E-05	9.87E-04	0.983	$O(F(x))O(\mathrm{NP}\cdot(T\varpi+1))$
	DE	4.452E-05	1.11E-03	1.108	$O(F(x))O(\mathrm{NP}\cdot(T\varpi+1))$

2023). The calculated values of T_0, T_1, and T_2 metrics (at K=100, NP=25, and T=1000) for modelling each system are listed in Table 4. Table 4 shows that the proposed ROA-based design took less runtime than other MVO-, BSO-, and DE-based design schemes.

4.2 System 3: nonlinear HW system identification using well-known models

The nonlinear block outputs ($g[n]$ and $y[n]$) of the HW system and its FIR filter transfer function $H(z)$ are given as follows (Scarpiniti et al., 2015b):

$$\begin{cases} g[n] = u[n] \Big/ \sqrt{0.1 + 0.9(u[n])^2}, \\ y[n] = q[n] - 0.5(q[n])^2 + 0.2(q[n])^3, \\ H(z) = 1 - 0.25z^{-1} + 0.05z^{-2} + 0.001z^{-3}. \end{cases} \quad (28)$$

In this study, the above HW system was identified using ROA along with different popular models such as the third-order Volterra model (Schetzen, 1981), Jeraj and Mathews model (Jeraj and Mathews, 2006), LNL model (Hegde et al., 2002a, 2002b), WSAF (Scarpiniti et al., 2013), HSAF (Scarpiniti et al., 2014), WH-SAF, and HW-SAF. Moreover, 1150 random input samples ($\in[-1, 1]$) were generated for system 3, in which a total of 1000 and 150 samples were allotted for the estimation and validation, respectively.

The actual and estimated outputs from the above models for system 3 from the validation data input are shown in Fig. 8a. It is apparent that the estimation results of all the models were close to the actual outputs. To show the deviation, a scatter plot was drawn using a few carefully chosen samples (Fig. 8b). Fig. 8b shows that the estimated output values of the HW-SAF and WH-SAF models were closer to the real ones. The fitness convergence plots for system 3 are shown in Fig. 8c. The approaches presented took 320 to 500 iterations to converge to their optimal solutions. The optimum fitness values obtained (after 1000 iterations) are given in Table 5. Moreover, the percentage of quality of fitness $\mathrm{QF}(\%) = \left(1 - \frac{1}{L}\sum_{n=1}^{L}(y[n]-\hat{y}[n])^2 \Big/ \left(\frac{1}{L}\sum_{n=1}^{L}(y[n])^2\right)\right) \times 100\%$ was evaluated. The measurement values for all approaches are reported in Table 5, and the measured QF was 90.22% and 92.65% using WH-SAF and HW-SAF models, respectively.

4.3 Real-time system identification

In this study, two real-time systems, namely, coupled electric drive system and thermic wall benchmark system, were identified using the ROA-based WH-SAF and HW-SAF models.

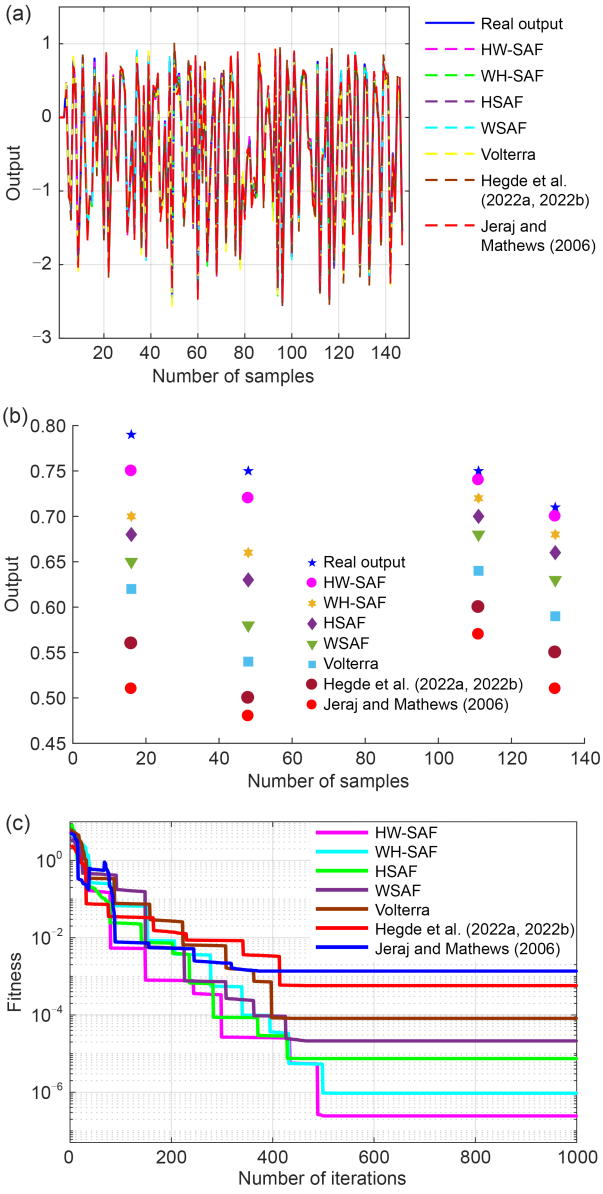

Fig. 8 Identification results of system 3 using different models based on the ROA method: (a) comparison of real and estimated outputs; (b) scatter plot for comparison of the estimated output values; (c) fitness convergence plot (References to colour refer to the online version of this figure)

Table 5 Fitness and QF metric comparison of different identification models for system 3

Method	Fitness	QF (%)
Jeraj and Mathews (2006)'s	1.33E-3	72.33
Hegde et al. (2002a, 2002b)'s	5.76E-4	74.78
Volterra	8.16E-5	79.24
WSAF	2.13E-5	81.33
HSAF	7.45E-6	87.59
WH-SAF	9.44E-7	90.22
HW-SAF	2.35E-7	92.65

4.3.1 System 4: coupled electric drive system identification

The basic details of the coupled electric drives (Wigren and Schoukens, 2013) are provided in the supplementary materials. Out of 500 input and output (I/O) samples, 400 I/O samples were chosen for estimation and 100 I/O samples for validation of the system (Fig. S7). We used ROA, MVO, BSO, and DE techniques to optimise the HW-SAF (with N=5, B-spline, and $\Delta u^{(1)}=\Delta u^{(2)}=0.2$) and WH-SAF (with $N_1=N_2=5$, B-spline, and $\Delta u=0.2$) structures for the estimation of system 4.

The secured optimum fitness and QF metric values for drive 1 and drive 2 datasets are listed in Table 6. Better results were achieved with the WH-SAF structure for all the techniques. Moreover, significantly improved results were achieved using ROA compared to MVO, BSO, and DE algorithms. Also, a slightly improved result was observed using the drive 2 dataset compared to the drive 1 dataset. The best fitness values for system 4 using the ROA-, MOA-, BSO-, and DE-based WH-SAF approaches were 8.33E-6, 1.37E-5, 3.66E-3, and 4.92E-2, respectively. Meanwhile, QF results of the respective algorithms were 92.52%, 90.45%, 86.21%, and 83.61%, respectively.

Table 6 Comparison of fitness and QF metric values of different identification models for system 4 using ROA, MVO, BSO, and DE techniques

Method	Metric	Drive 1		Drive 2	
		WH-SAF	HW-SAF	WH-SAF	HW-SAF
ROA	Fitness	7.28E-5	6.38E-4	8.33E-6	1.64E-5
	QF (%)	91.87	90.56	93.76	92.52
MVO	Fitness	2.62E-3	7.66E-3	1.37E-5	3.56E-4
	QF (%)	88.46	87.12	91.45	90.45
BSO	Fitness	3.33E-2	9.67E-2	3.66E-3	7.34E-3
	QF (%)	85.32	83.95	87.56	86.21
DE	Fitness	9.55E-2	3.57E-1	4.92E-2	2.78E-2
	QF (%)	82.67	80.75	84.47	83.61

Fig. 9a shows the validation results using the proposed RSA-based design for the drive 1 and drive 2 datasets. The WH-SAF-based estimated output was nearer to the actual output than the HW-SAF-based one. The convergence of fitness values for drive 1 and drive 2 datasets for system 4 using the proposed RSA-based design is shown in Fig. 9b. Both models took around 290 to 340 iterations for convergence.

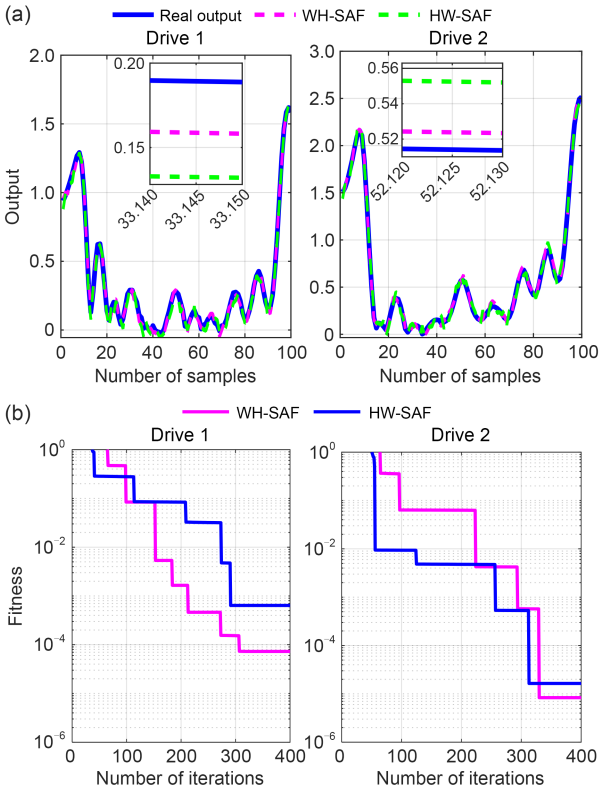

Fig. 9 Identification results of system 4 (coupled electric drive system) using different models based on ROA for the drive 1 and drive 2 datasets: (a) validation outputs; (b) fitness convergence (References to colour refer to the online version of this figure)

4.3.2 System 5: thermic wall system identification

This study identified the thermic wall system by taking the input (external temperature) and output (heat flow density) datasets from the Daisy database (De Moor, 2004). From a total of 1680 samples, 1200 and 480 data samples were used for estimation and validation purposes, respectively (Fig. 10a).

The fitness and QF metric results obtained for system 5 modelling using ROA, MVO, BSO, and DE techniques are shown in Table 7. The best fitness and QF metric results achieved from the proposed ROA were 3.43E-5 and 92.65%, respectively. Meanwhile, the nearest competitor (MVO) produced a fitness of 2.75E-4 and QF of 90.13%. Finally, DE gave significantly lower quality results (fitness of 4.67 and QF of 81.76%) than others. The results achieved for validation outputs and convergence speed of the fitness

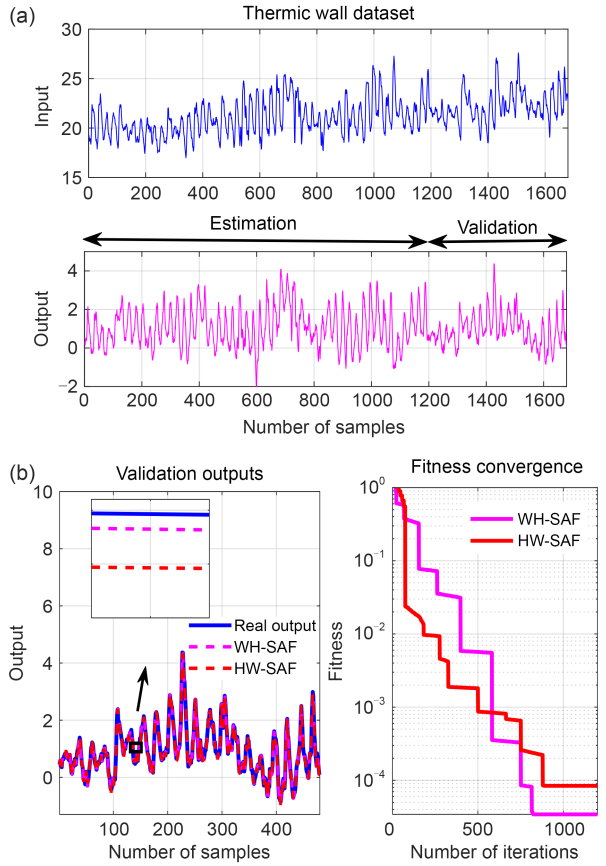

Fig. 10 Identification results of system 5 (thermic wall system) using different models based on ROA: (a) I/O datasets (De Moor, 2004); (b) comparison of validation outputs and fitness convergence (References to colour refer to the online version of this figure)

Table 7 Comparison of fitness and QF metrics of different identification models for system 5

Method	Metric	WH-SAF	HW-SAF
ROA	Fitness	3.43E-5	8.41E-5
	QF (%)	92.65	91.72
MVO	Fitness	2.75E-4	6.67E-4
	QF (%)	90.13	89.16
BSO	Fitness	1.56E-2	7.83E-2
	QF (%)	86.45	85.33
DE	Fitness	4.67	9.95
	QF (%)	81.76	80.42

function for the thermic wall system by the proposed ROA-based HW-SAF and WH-SAF models are shown in Fig. 10b. From Fig. 10b, the presented schemes exhibited good tracking accuracy and achieved the best fitness values with the WH-SAF and HW-SAF models after 810 and 892 iterations, respectively.

4.3.3 System 6: CSTR plant estimation

Details of the CSTR plant and its datasets are briefly discussed in the supplementary materials. To model CSTR using the HW-SAF and WH-SAF models, the actual input coolant flow rate $q_c(t)$ and output concentration $C_A(t)$ (Lightbody and Irwin, 1997; Hafezi and Arefi, 2019; Janjanam et al., 2022d) datasets were collected from the Daisy database (De Moor, 2004). The achieved fitness and QF metric results for system 6 using all the algorithms for both structures are presented in Table 8. The WH-SAF model showed superior performance compared to the HW-SAF model. The best fitness values achieved for ROA, MVO, BSO, and DE methods were 1.45E-4, 2.36E-3, 4.58E-1, and 6.49, respectively. In comparison, QF metric results of the respective algorithms were 90.36%, 88.66%, 84.32%, and 80.35%, respectively. The fitness convergence behaviour for the best algorithm (ROA) with WH-SAF and HW-SAF structures for the CSTR system modelling is depicted in Fig. 11a and the optimal fitness function values are achieved after 616 and 771 iterations, respectively. We derived the estimated output using the optimised WH-SAF model and the validation data input samples, closely tracking the actual output (Fig. 11b).

Table 8 Comparison of fitness and QF metrics of different identification models for system 6

Method	Metric	WH-SAF	HW-SAF
ROA	Fitness	1.45E-4	8.36E-4
	QF (%)	90.36	89.65
MVO	Fitness	2.36E-3	6.73E-3
	QF (%)	88.66	87.53
BSO	Fitness	4.58E-1	9.67E-2
	QF (%)	84.32	83.21
DE	Fitness	6.49	8.65
	QF (%)	80.35	79.33

5 Conclusions and future directions

In this study, two recently proposed novel CSAFs, WH-SAF and HW-SAF, were effectively identified using the ROA technique. ROA optimises spline control points and linear filter coefficients jointly using the formulated objective function, enhancing performance stability. The comparative study of competent algorithms, such as MVO, BSO, and DE, for the exact

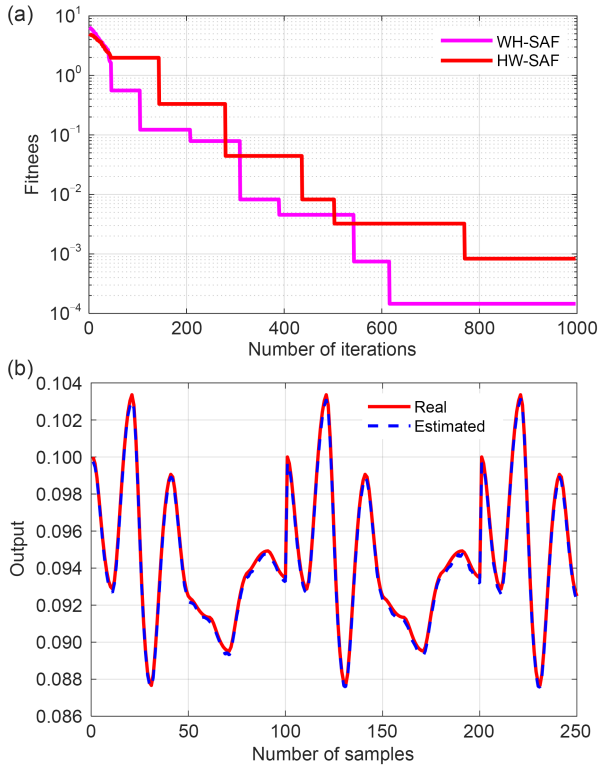

Fig. 11 CSTR plant identification results using ROA: (a) fitness convergence behaviour; (b) real and estimated outputs (References to colour refer to the online version of this figure)

problem identification, revealed that the proposed ROA-based scheme yields highly accurate estimated parameters with higher convergence speed. The statistical results of numerous performance indices and the performance comparison of algorithms under various noise levels σ^2=0.001^2, 0.01^2, and 0.1^2 confirmed that the proposed design approach is more statistically significant, reliable, robust, and stable than the others. The results of the statistical hypothesis test showed that the ROA- and DE-based schemes had more consistent performance than MVO- and BSO-based approaches. However, the DE scheme provided substantially lower quality results than the others. Moreover, various attractive models were applied for designing a nonlinear HW system, which yielded significantly improved results using WH-SAF and HW-SAF models. Additionally, the estimation results of coupled electric drives, thermic wall systems, and CSTR showed the real strength of the proposed ROA-based CSAF design approach in a practical scenario.

For future scope, the proposed method will be extended to multiple-input and multiple-output systems and will be used to solve the estimation problems of multi-dimensional real-time nonlinear plants.

Contributors

Lakshminarayana JANJANAM contributed to the conceptualization, methodology, software development, and the draft of the paper. Suman Kumar SAHA helped organise the paper and was responsible for the data curation. Rajib KAR provided the visualization, conducted the investigations, supervised the project, and revised and finalised the paper.

Conflict of interest

All the authors declare that they have no conflict of interest.

Data availability

The data that support the findings of this study are available from the corresponding author upon reasonable request.

References

Braik M, Hammouri A, Atwan J, et al., 2022. White shark optimizer: a novel bio-inspired meta-heuristic algorithm for global optimization problems. *Knowl-Based Syst*, 243: 108457. https://doi.org/10.1016/j.knosys.2022.108457

Chaudhary NI, Manzar MA, Raja MAZ, 2019. Fractional Volterra LMS algorithm with application to Hammerstein control autoregressive model identification. *Neur Comput Appl*, 31(9):5227-5240. https://doi.org/10.1007/s00521-018-3362-z

Chen ZY, Meng YH, Chen T, 2022. NN model-based evolved control by DGM model for practical nonlinear systems. *Expert Syst Appl*, 193:115873. https://doi.org/10.1016/j.eswa.2021.115873

De Moor B, 2004. Database for Identification of Systems. https://homes.esat.kuleuven.be/~smc/~daisy/ [Accessed on Nov. 15, 2023].

Esmaeilani L, Ghaisari J, Bagherzadeh MA, 2021. Hammerstein–Wiener identification of industrial plants: a pressure control valve case study. *IET Contr Theory Appl*, 15(3): 416-431. https://doi.org/10.1049/cth2.12052

Gao Y, Zhao HQ, Zhu YY, et al., 2023. Spline adaptive filtering algorithm-based generalized maximum correntropy and its application to nonlinear active noise control. *Circ Syst Signal Process*, 42(11):6636-6659. https://doi.org/10.1007/s00034-023-02411-5

Gao Y, Zhao HQ, Zhu YY, et al., 2024. The q-gradient LMS spline adaptive filtering algorithm and its variable step-size variant. *Inform Sci*, 658:119983. https://doi.org/10.1016/j.ins.2023.119983

Garcia-Vega S, Zeng XJ, Keane J, 2020. Stock returns prediction using kernel adaptive filtering within a stock market interdependence approach. *Expert Syst Appl*, 160:113668. https://doi.org/10.1016/j.eswa.2020.113668

Guan SH, Biswal B, 2023. Spline adaptive filtering algorithm based on different iterative gradients: performance analysis and comparison. *J Autom Intell*, 2(1):1-13.

https://doi.org/10.1016/j.jai.2022.100008

Guan SH, Cheng Q, Zhao Y, et al., 2022. Spline adaptive filtering algorithm based on Heaviside step function. *Signal Image Video Process*, 16(5):1333-1343. https://doi.org/10.1007/s11760-021-02085-z

Guo WY, Zhi YF, 2022. Nonlinear spline adaptive filtering against non-Gaussian noise. *Circ Syst Signal Process*, 41(1): 579-596. https://doi.org/10.1007/s00034-021-01798-3

Guo WY, Zhi YF, Feng K, 2022. Nonlinear spline prioritization optimization adaptive filter with arctangent-exponential hyperbolic cosine. *Nonl Dynam*, 110(1):611-621. https://doi.org/10.1007/s11071-022-07636-8

Hafezi Z, Arefi MM, 2019. Recursive generalized extended least squares and RML algorithms for identification of bilinear systems with ARMA noise. *ISA Trans*, 88:50-61. https://doi.org/10.1016/j.isatra.2018.12.015

Hammar K, Djamah T, Bettayeb M, 2019. Nonlinear system identification using fractional Hammerstein–Wiener models. *Nonl Dynam*, 98(3):2327-2338. https://doi.org/10.1007/s11071-019-05331-9

Hegde V, Radhakrishnan C, Krusienski DJ, et al., 2002a. Architectures and algorithms for nonlinear adaptive filters. 36th Asilomar Conf on Signals, Systems and Computers, p.1015-1018. https://doi.org/10.1109/ACSSC.2002.1196937

Hegde V, Radhakrishnan C, Krusienski D, et al., 2002b. Series-cascade nonlinear adaptive filters. 45th Midwest Symp on Circuits and Systems, p.III-219-III-222. https://doi.org/10.1109/MWSCAS.2002.1187010

Holm S, 1979. A simple sequentially rejective multiple test procedure. *Scand J Stat*, 6(2):65-70.

Janjanam L, Saha SK, Kar R, et al., 2021a. An efficient identification approach for highly complex non-linear systems using the evolutionary computing method based Kalman filter. *AEU Int J Electron Commun*, 138:153890. https://doi.org/10.1016/j.aeue.2021.153890

Janjanam L, Saha SK, Kar R, et al., 2021b. Global gravitational search algorithm-aided Kalman filter design for Volterra-based nonlinear system identification. *Circ Syst Signal Process*, 40(5):2302-2334. https://doi.org/10.1007/s00034-020-01593-6

Janjanam L, Saha SK, Kar R, et al., 2022a. Hammerstein-Wiener nonlinear system identification by using honey badger algorithm hybridized Sage-Husa adaptive Kalman filter with real-time applications. *AEU Int J Electron Commun*, 151: 154218. https://doi.org/10.1016/j.aeue.2022.154218

Janjanam L, Saha SK, Kar R, et al., 2022b. Improving the modelling efficiency of Hammerstein system using Kalman filter and its parameters optimised using social mimic algorithm: application to heating and cascade water tanks. *J Franklin Inst*, 359(3):1239-1273. https://doi.org/10.1016/j.jfranklin.2021.12.022

Janjanam L, Saha SK, Kar R, et al., 2022c. Optimal design of cascaded Wiener-Hammerstein system using a heuristically supervised discrete Kalman filter with application on benchmark problems. *Expert Syst Appl*, 200:117065. https://doi.org/10.1016/j.eswa.2022.117065

Janjanam L, Saha SK, Kar R, et al., 2022d. Wiener model-based system identification using moth flame optimised Kalman filter algorithm. *Signal Image Video Process*, 16(5): 1425-1433. https://doi.org/10.1007/s11760-021-02096-w

Janjanam L, Saha SK, Kar R, 2023. Optimal design of Hammerstein cubic spline filter for nonlinear system modeling based on snake optimiser. *IEEE Trans Ind Electron*, 70(8): 8457-8467. https://doi.org/10.1109/TIE.2022.3213886

Jeraj J, Mathews VJ, 2006. A stable adaptive Hammerstein filter employing partial orthogonalization of the input signals. *IEEE Trans Signal Process*, 54(4):1412-1420. https://doi.org/10.1109/TSP.2006.870643

Jia HM, Lang CB, Oliva D, et al., 2019. Dynamic Harris hawks optimization with mutation mechanism for satellite image segmentation. *Remote Sens*, 11(12):1421. https://doi.org/10.3390/rs11121421

Jia HM, Peng XX, Lang CB, 2021. Remora optimization algorithm. *Expert Syst Appl*, 185:115665. https://doi.org/10.1016/j.eswa.2021.115665

Jia HM, Rao HH, Wen CS, et al., 2023. Crayfish optimization algorithm. *Artif Intell Rev*, 56(2):1919-1979. https://doi.org/10.1007/s10462-023-10567-4

Jia L, Feng QL, 2017. Combined separable signals based neuro-fuzzy Hammerstein–Wiener model. *Memet Comput*, 9(3): 245-259. https://doi.org/10.1007/s12293-016-0204-3

Li LW, Ren XM, 2018. Identification of nonlinear Wiener-Hammerstein systems by a novel adaptive algorithm based on cost function framework. *ISA Trans*, 80:146-159. https://doi.org/10.1016/j.isatra.2018.07.015

Li WQ, Xu M, Tang JS, et al., 2023. Robust frequency domain spline adaptive filtering based on the half-quadratic criterion: performance analysis and applications. *IEEE Trans Instrum Meas*, 72:6503513. https://doi.org/10.1109/TIM.2023.3271721

Lightbody G, Irwin GW, 1997. Nonlinear control structures based on embedded neural system models. *IEEE Trans Neur Netw*, 8(3):553-567. https://doi.org/10.1109/72.572095

Liu C, Zhao HQ, 2023. A 2D-LUT scheme design for complex-valued spline adaptive filter. *IEEE Trans Circ Syst II Expr Briefs*, 70(8):3154-3158. https://doi.org/10.1109/TCSII.2023.3245670

Liu Q, Tang XM, Li JH, et al., 2021. Identification of Wiener–Hammerstein models based on variational Bayesian approach in the presence of process noise. *J Franklin Inst*, 358(10):5623-5638. https://doi.org/10.1016/j.jfranklin.2021.05.003

Mehmood A, Raja MAZ, 2023. Novel design of weighted differential evolution for parameter estimation of Hammerstein-Wiener systems. *J Adv Res*, 43:123-136. https://doi.org/10.1016/j.jare.2022.02.010

Mehmood A, Zameer A, Chaudhary NI, et al., 2019a. Backtracking search heuristics for identification of electrical muscle stimulation models using Hammerstein structure. *Appl Soft Comput*, 84:105705. https://doi.org/10.1016/j.asoc.2019.105705

Mehmood A, Chaudhary NI, Zameer A, et al., 2019b. Backtracking search optimization heuristics for nonlinear Hammerstein controlled auto regressive auto regressive systems. *ISA Trans*, 91:99-113. https://doi.org/10.1016/j.isatra.2019.01.042

Mirjalili S, Lewis A., 2016. The whale optimization algorithm. *Adv Eng Softw*, 95:51-67. https://doi.org/10.1016/j.advengsoft.2016.01.008

Mirjalili S, Mirjalili SM, Hatamlou A, 2016. Multi-verse optimizer: a nature-inspired algorithm for global optimization. *Neur Comput Appl*, 27(2):495-513. https://doi.org/10.1007/s00521-015-1870-7

Mishra BP, Panigrahi T, Wilson AM, et al., 2023. Nonlinear channel estimation based on robust distributed Hammerstein spline adaptive technique in wireless sensor network. *Dig Signal Process*, 132:103791. https://doi.org/10.1016/j.dsp.2022.103791

Nayak C, Saha SK, Kar R, et al., 2019. An efficient and robust digital fractional order differentiator based ECG preprocessor design for QRS detection. *IEEE Trans Biomed Circ Syst*, 13(4):682-696. https://doi.org/10.1109/TBCAS.2019.2916676

Pal PS, Kar R, Mandal D, et al., 2017. Parametric identification with performance assessment of Wiener systems using brain storm optimization algorithm. *Circ Syst Signal Process*, 36(8):3143-3181. https://doi.org/10.1007/s00034-016-0464-7

Patel V, Gandhi V, Heda S, et al., 2016. Design of adaptive exponential functional link network-based nonlinear filters. *IEEE Trans Circ Syst I Reg Pap*, 63(9):1434-1442. https://doi.org/10.1109/TCSI.2016.2572091

Raja MAZ, Aslam MS, Chaudhary NI, et al., 2018. Bio-inspired heuristics hybrid with interior-point method for active noise control systems without identification of secondary path. *Front Inform Technol Electron Eng*, 19(2):246-259. https://doi.org/10.1631/FITEE.1601028

Sankar S, Kar A, Burra S, et al., 2020. Nonlinear acoustic echo cancellation with kernelized adaptive filters. *Appl Acoust*, 166:107329. https://doi.org/10.1016/j.apacoust.2020.107329

Scarpiniti M, Comminiello D, Parisi R, et al., 2013. Nonlinear spline adaptive filtering. *Signal Process*, 93(4):772-783. https://doi.org/10.1016/j.sigpro.2012.09.021

Scarpiniti M, Comminiello D, Parisi R, et al., 2014. Hammerstein uniform cubic spline adaptive filters: learning and convergence properties. *Signal Process*, 100:112-123. https://doi.org/10.1016/j.sigpro.2014.01.019

Scarpiniti M, Comminiello D, Parisi R, et al., 2015a. Nonlinear system identification using IIR spline adaptive filters. *Signal Process*, 108:30-35. https://doi.org/10.1016/j.sigpro.2014.08.045

Scarpiniti M, Comminiello D, Parisi R, et al., 2015b. Novel cascade spline architectures for the identification of nonlinear systems. *IEEE Trans Circ Syst I Reg Pap*, 62(7):1825-1835. https://doi.org/10.1109/TCSI.2015.2423791

Scarpiniti M, Comminiello D, Parisi R, et al., 2018. Spline adaptive filters: theory and applications. In: Comminiello D, Príncipe JC (Eds.), Adaptive Learning Methods for Nonlinear System Modeling. Elsevier, Amsterdam, the Netherlands, p.47-69. https://doi.org/10.1016/B978-0-12-812976-0.00004-X

Schetzen M, 1981. Nonlinear system modeling based on the Wiener theory. *Proc IEEE*, 69(12):1557-1573. https://doi.org/10.1109/PROC.1981.12201

Shadravan S, Naji HR, Bardsiri VK, 2019. The sailfish optimizer: a novel nature-inspired metaheuristic algorithm for solving constrained engineering optimization problems. *Eng Appl Artif Intell*, 80:20-34. https://doi.org/10.1016/j.engappai.2019.01.001

Shi YH, 2011. Brain storm optimization algorithm. Proc 2nd Int Conf on Advances in Swarm Intelligence, p.303-309. https://doi.org/10.1007/978-3-642-21515-5_36

Storn R, Price K, 1997. Differential evolution—a simple and efficient heuristic for global optimization over continuous spaces. *J Glob Optim*, 11(4):341-359. https://doi.org/10.1023/A:1008202821328

Wang YJ, Tang SH, Gu XB, 2022. Parameter estimation for nonlinear Volterra systems by using the multi-innovation identification theory and tensor decomposition. *J Franklin Inst*, 359(2):1782-1802. https://doi.org/10.1016/j.jfranklin.2021.11.015

Wigren T, Schoukens J, 2013. Three free data sets for development and benchmarking in nonlinear system identification. European Control Conf, p.2933-2938. https://doi.org/10.23919/ECC.2013.6669201

Xu L, Jia HM, Lang CB, et al., 2019. A novel method for multilevel color image segmentation based on dragonfly algorithm and differential evolution. *IEEE Access*, 7:19502-19538. https://doi.org/10.1109/ACCESS.2019.2896673

Yadav S, Saha SK, Kar R, et al., 2022. EEG/ERP signal enhancement through an optimally tuned adaptive filter based on marine predators algorithm. *Biomed Signal Process Contr*, 73:103427. https://doi.org/10.1016/j.bspc.2021.103427

Yadav S, Saha SK, Kar R, 2023. An application of the Kalman filter for EEG/ERP signal enhancement with the autoregressive realisation. *Biomed Signal Process Contr*, 86:105213. https://doi.org/10.1016/j.bspc.2023.105213

Yan H, Zhong CQ, Wu YH, et al., 2023. A hybrid-model optimization algorithm based on the Gaussian process and particle swarm optimisation for mixed-variable CNN hyperparameter automatic search. *Front Inform Technol Electron Eng*, 24(11):1557-1573. https://doi.org/10.1631/FITEE.2200515

Yang LD, Liu JX, Yan RQ, et al., 2019. Spline adaptive filter with arctangent-momentum strategy for nonlinear system identification. *Signal Process*, 164:99-109. https://doi.org/10.1016/j.sigpro.2019.06.007

Yu T, Li WQ, Yu Y, et al., 2021. Robust spline adaptive filtering based on accelerated gradient learning: design and performance analysis. *Signal Process*, 183:107965. https://doi.org/10.1016/j.sigpro.2021.107965

Yu T, Tan SJ, Li WQ, et al., 2024. Performance analysis of robust subband Hammerstein spline adaptive filter. *Circ Syst Signal Process*, 43(1):368-387. https://doi.org/10.1007/s00034-023-02476-2

Zhang YF, Zhao ZD, Deng YJ, et al., 2021. ECGID: a human identification method based on adaptive particle swarm optimization and the bidirectional LSTM model. *Front Inform Technol Electron Eng*, 22(12):1641-1654. https://doi.org/10.1631/FITEE.2000511

List of supplementary materials

1 A pictorial representation of the mathematical analysis HW-SAF modelling

2 The pseudocode of the proposed ROA-based CSAF design

3 Justification for the choice of common control parameter values

4 Parameter convergence profiles of system 2 using the ROA method

5 AE metric results for system 2 using the ROA, MVO, BSO, and DE algorithms under different noise variance levels

6 Comparison of the performance of the techniques used for system 2 based on various performance indices

7 Fitness convergence profiles for system 2

8 Percentage improvement resulting from the use of the proposed algorithm over others for systems 1 and 2

9 Statistical results of the estimated parameters of system 2

10 Statistical analysis of the global metric results for system 2

11 Fitness metric results from 100 independent runs of the algorithms used for system 2

12 Holm's consistency test

13 Proof of $O(\mathrm{MOA}) = O(F(x))O(\mathrm{NP}\cdot(T\varpi+1))$

14 Basic details of the coupled electric drive system

15 Basic details of the CSTR system

Fig. S1 Implementation of the proposed ROA-based HW-SAF design

Fig. S2 Parameter convergence profiles of system 2 for the best run of ROA technique

Fig. S3 AE metric results for system 2 using the ROA, MVO, BSO, and DE algorithms under different noise variance levels

Fig. S4 Fitness convergence profiles for system 2 using the ROA, MVO, BSO, and DE algorithms under different noise levels

Fig. S5 Improvement of the proposed ROA-based design compared to MVO-, BSO-, and DE-based designs for systems 1 and 2 with the noise level of $\sigma^2=0.001^2$ in terms of different metrics

Fig. S6 Independent run results of fitness metric for system 2 using the considered algorithms under different noise levels

Fig. S7 Identification results of system 4 (coupled electric drive system) using different models based on ROA

Fig. S8 CSTR practical plant identification results using ROA

Table S1 Pseudocode of the proposed ROA-based CSAF design

Table S2 Comparison of various performance indices for the employed techniques used for system 2

Table S3 Statistical results of the estimated parameters of system 2 using the chosen algorithms under the noise level of $\sigma^2=0.001^2$

Table S4 Statistical analysis of the global metric results for system 2 using the chosen algorithms under different noise levels

Table S5 Holm's test for the employed algorithms for systems 1 and 2